Colloquium: Spintronics in graphene and other two-dimensional materials

A. Avsar

Electrical Engineering Institute and Institute of Materials Science and Engineering, École Polytechnique Fédérale de Lausanne (EPFL), Lausanne CH-1015, Switzerland

H. Ochoa

Department of Physics, Columbia University, New York, New York 10027, USA

F. Guinea

Imdea Nanociencia, Faraday 9, 28049 Madrid, Spain, Department of Physics and Astronomy, University of Manchester, Manchester M13 9PL, United Kingdom, and Donostia International Physics Center, Paseo Manuel de Lardizabal 4, 20018 San Sebastian, Spain

B. Özyilmaz

Department of Physics, National University of Singapore, Singapore 117542, Singapore, Centre for Advanced 2D Materials, National University of Singapore, Singapore 117546, Singapore, and Department of Materials Science and Engineering, National University of Singapore, Singapore 117575, Singapore

B. J. van Wees*

Physics of Nanodevices, Zernike Institute for Advanced Materials, University of Groningen, Nijenborgh 4, 9747 AG Groningen, Netherlands

I. J. Vera-Marun†

Department of Physics and Astronomy, University of Manchester, Manchester M13 9PL, United Kingdom and National Graphene Institute, University of Manchester, Manchester M13 9PL, United Kingdom

(published 2 June 2020)

After the first unequivocal demonstration of spin transport in graphene [Tombros *et al.*, Nature (London) **448**, 571–574 (2007)], surprisingly at room temperature, it was quickly realized that this novel material was relevant for both fundamental spintronics and future applications. In the decade since, exciting results have made the field of graphene spintronics blossom, and a second generation of studies has extended to new two-dimensional (2D) compounds. This Colloquium reviews recent theoretical and experimental advances on electronic spin transport in graphene and related 2D materials, focusing on emergent phenomena in van der Waals heterostructures and the new perspectives provided by them. These phenomena include proximity-enabled spin-orbit effects, the coupling of electronic spin to light, electrical tunability, and 2D magnetism.

DOI: 10.1103/RevModPhys.92.021003

CONTENTS

*b.j.van.wees@rug.nl
†ivan.veramarun@manchester.ac.uk

I. INTRODUCTION

In 1988, A. Fert and P. Grunberg independently discovered that the resistance of ferromagnetic/nonmagnetic (FM/NM) metallic multilayers depends on the relative orientation of the FM layers (Baibich *et al.*, 1988; Binasch *et al.*, 1989). This discovery, termed giant magnetoresistance (GMR), was soon utilized in the magnetic field sensors of hard disk drives (Tsang *et al.*, 1998), constituting the first major application of spintronics within modern electronics. The physics behind this achievement has formed the foundation of spin-transport experiments and their evolution over the past three decades (Fert, 2008).

Spintronics aims to utilize the spin degree of freedom to complement or replace charge as the information carrier for high speed, low-power computing (Wolf, Chtchelkanova, and Treger, 2006). The drive for this use of spin-polarized transport started with the proposal of the Datta-Das spin field-effect transistor, which relies on the electrical manipulation of spin information during its propagation in a nonmagnetic channel (Datta and Das, 1990). This was followed by other proposals of integrating magnetic semiconductors into spin-based diodes and transistors (Flatté and Vignale, 2001), and ultimately all-spin logic circuits with built-in memory (Behin-Aein *et al.*, 2010). These proposals led to major experimental advances, including the demonstration of spin injection, transport, and detection in metals (Jedema, Filip, and van Wees, 2001) and semiconductors (Lou *et al.*, 2007). The latter offers the prospect of harnessing the spin degree of freedom for quantum storage and computation (Awschalom, Loss, and Samarth, 2002; Flatté, 2007). Despite these initial successes, most of those earlier concepts have not been experimentally realized. The reason for this is that an ideal material platform capable of transporting spin information over long distances at room temperature was still lacking.

Since the discovery of graphene, the field of two-dimensional (2D) materials has become one of the most active areas of research in solid-state physics, mainly because of their prominent mechanical, optical, electrical, and magnetic properties (Castro Neto *et al.*, 2009; Novoselov, 2011). High electronic charge mobility, low spin-orbit coupling strength, negligible hyperfine interaction, and gate tunability are some of the properties that have established graphene as an emerging material for spintronics (Tombros *et al.*, 2007). Graphene exhibits the longest spin-relaxation length ever measured at room temperature (Ingla-Aynés *et al.*, 2015; Drögeler *et al.*, 2016). This property enables the transmission and manipulation of spin signals within complex multiterminal device architectures (Kamalakar, Groenveld *et al.*, 2015; Gebeyehu *et al.*, 2019). Recently the field has moved beyond only graphene-based devices toward exploring the properties of other 2D crystals and their heterostructures, which serve as test beds for inducing emergent functionalities, see Fig. 1. The observation of long spin-relaxation lengths (Drögeler *et al.*, 2016) together with spin-charge conversion (Safeer *et al.*, 2019) and spin manipulation (Avsar, Tan *et al.*, 2017) capabilities in van der Waals heterostructures makes 2D crystals appealing material systems for the development of low-power spintronics devices. The latter include, among others, devices based on tunnel magnetoresistance (Kim *et al.*, 2018), spin-transfer torque (Lin *et al.*, 2013), and spin logic gates (Wen *et al.*, 2016).

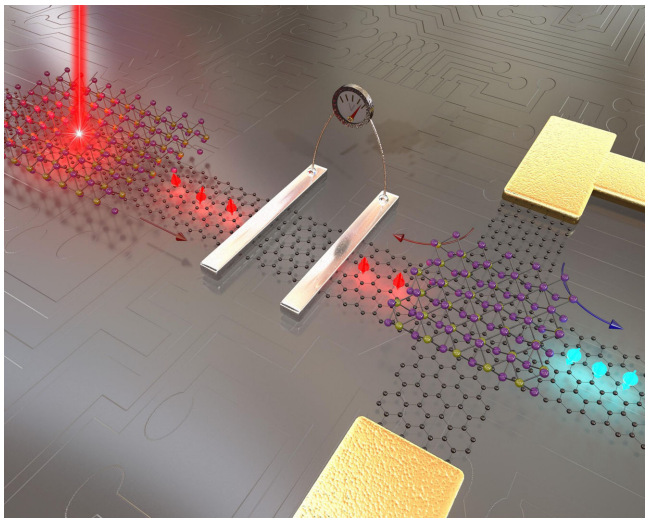

FIG. 1. Illustration of emergent spintronic phenomena in a 2D van der Waals heterostructure. Graphene acts as an ideal spin-transport channel given its long spin-relaxation length. In the center of the channel two magnetic contacts are used to electrically inject or detect the spin current. The need for magnetic contacts is circumvented by using heterostructures of graphene and transition-metal dichalcogenides, which enable direct optical spin injection (top left) and direct charge-to-spin conversion (bottom right).

Given the increasing effort on the search for new spintronics phenomena in 2D materials, there is presently a need for a review and critical discussion of recent experimental and theoretical progress within the field of 2D spintronics. We note that there are relevant reviews on spin transport (Meservey and Tedrow, 1994; Žutić, Fabian, and Das Sarma, 2004; Wolf, Chtchelkanova, and Treger, 2006; Chappert, Fert, and Van Dau, 2007), graphene (Castro Neto *et al.*, 2009; Peres, 2010; Das Sarma *et al.*, 2011), and graphene spintronics (Han *et al.*, 2012; Pesin and MacDonald, 2012; Seneor *et al.*, 2012; Shiraishi, 2012; Roche and Valenzuela, 2014; Roche *et al.*, 2015; Garcia *et al.*, 2018; Gurram, Omar, and van Wees, 2018; Žutić *et al.*, 2019; Dayen *et al.*, 2020). Our aim in this Colloquium is to offer broad and balanced coverage, starting with an introduction to fundamentals for

those new to the fields of spintronics and graphene, while encompassing critical discussions that address recent advances and point to challenges and future directions in this vibrating field. While brief discussions on chemically modified graphene and alternative spin injection schemes will be provided, this Colloquium focuses primarily on electronic spin transport in pristine 2D materials and novel devices based on their heterostructures.

A. Initial spin-transport experiments

At the heart of most spin-transport phenomena is the creation of spin accumulation in a NM material. The latter can be electrically induced by applying a charge current to the NM via a FM contact. The injected spin information propagates throughout the NM as a spin current, which can be detected using a second FM contact. Such detection is possible as long as the separation between the injector and detector contacts is less than the characteristic length on which the nonequilibrium spin information relaxes. Within these conditions, the resistance of the device depends on the relative magnetization direction of the injector and detector contacts, which is detected as a resistance switch when their relative orientation changes from the parallel to the antiparallel (Johnson and Silsbee, 1985; Jedema, Filip, and van Wees, 2001). Such a spin valve signal in FM/NM/FM structures is therefore utilized for the realization of spin injection, spin transport, and spin detection. In this local architecture, the charge and spin currents are colocated within the same NM channel. The measured signal is therefore a combination of a spin-dependent resistance, representative of the spin transport, and a spin-independent resistance, purely associated with charge transport. Since the ratio of the spin-dependent resistance to the spin-independent resistance is generally small and charge-based phenomena can mimic the spin signal under study, this two-terminal measurement geometry is not ideal for probing spin-dependent transport.

Multiterminal measurement geometries are thus favored for the unambiguous study of spin-dependent transport; see Fig. 2. One alternative is the three-terminal Hanle geometry, where a single magnetic contact is used to create and detect spin accumulation. The latter is evidenced by the modulation of the contact resistance due to the spin precession effect of an applied magnetic field. This measurement configuration has advantages for probing spin lifetimes in highly resistive channel materials or in materials with a short spin-relaxation length, and it has been utilized to detect spin injection in GaAs (Lou *et al.*, 2006, 2007), Si (Dash *et al.*, 2009), and Ge (Jeon *et al.*, 2011). However, a disadvantage of this configuration is that the same contact is used to electrically inject and detect the spin information, which does not fully solve the issue of mixing charge and spin phenomena, as evidenced in measurements showing spin accumulations that are inconsistent with the theoretical expectations (Tran *et al.*, 2009). Therefore, the ideal method is that of a four-terminal nonlocal geometry; see Fig. 2. This nonlocal geometry has been widely utilized to spatially separate the paths of the charge current and the detected spin current, providing a reliable measurement of

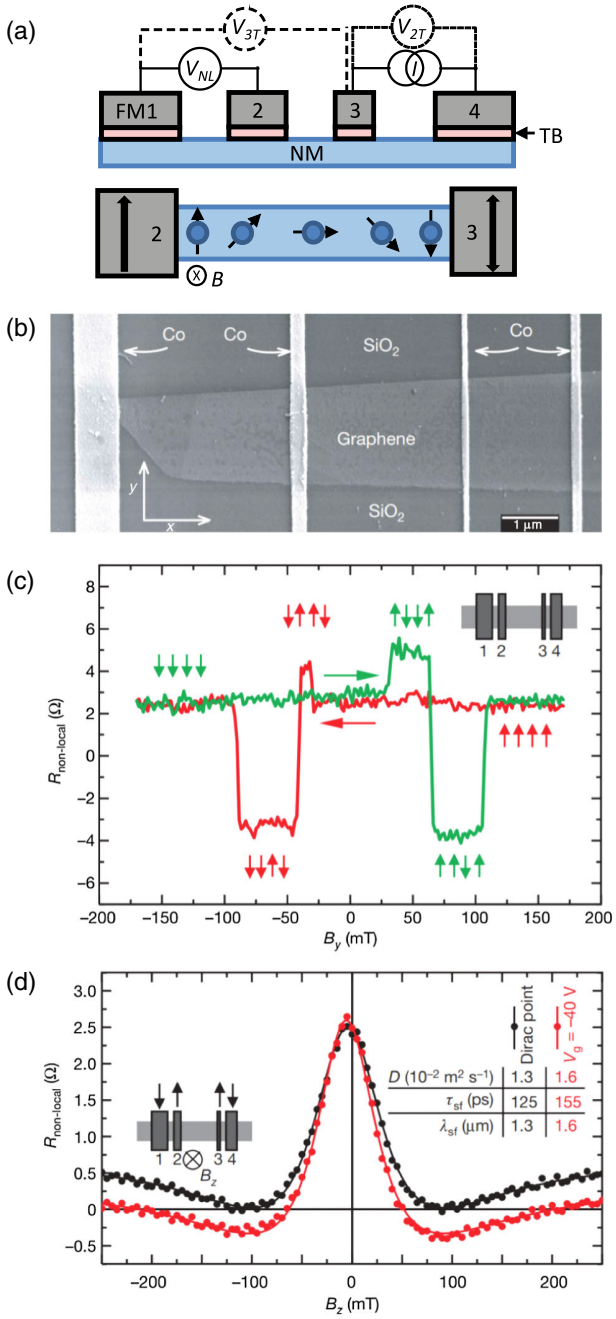

FIG. 2. Measurement configurations and spin transport in graphene. (a) Four-terminal nonlocal (V_{NL}), three-terminal Hanle (V_{3T}), and two-terminal local (V_{2T}) measurement geometries. Ferromagnetic (FM) contacts are used to inject and detect spins in a nonmagnetic (NM) channel via a tunnel barrier (TB). The bottom sketch illustrates a top view of spin precession under an out-of-plane applied magnetic field B. (b) Scanning electron micrograph of the first nonlocal graphene spin valve device. (c) Nonlocal spin valve signal in monolayer graphene. Vertical arrows represent the polarization direction of the contacts, and lateral arrows represent the magnetic field sweep direction. (d) Corresponding Hanle spin precession signal, for parallel orientation of the contacts. Adapted from Tombros *et al.*, 2007.

spin-dependent transport. This method relies on the detection of pure spin current and was first established for metallic spin valves (Johnson and Silsbee, 1985; Jedema, Filip, and van

Wees, 2001) and later also applied to semiconductor-based devices (Lou *et al.*, 2007).

Quantitative extraction of the parameters that control spin transport in a diffusive channel, namely, the spin-relaxation time τ_s and the spin diffusion coefficient D_s, can be achieved by measuring the dependence of the spin signal on the separation between the injector and detector electrodes. The observed decay with increasing separation yields the spin-relaxation length $\lambda_s = \sqrt{D_S \tau_s}$, while D_s can be calculated from the resistivity via the Einstein relation (Jedema, Filip, and van Wees, 2001). Nevertheless, this requires the study of multiple devices with different separation and is sensitive to the reproducibility of other parameters, like the spin injection efficiency of the contacts, which also control the magnitude of the spin signal. Hanle spin precession is an alternative measurement based on studying the dependence of the spin signal on an applied magnetic field B perpendicular to the orientation of the injected spin (Jedema, Heersche *et al.*, 2002). Here a torque is exerted on the electron spin, which is forced to precess at the Larmor frequency, as sketched in Fig. 2(a). In a fully coherent 1D channel, the spin precession leads to an oscillatory response as a function of B. Nevertheless, in a diffusive 2D or 3D channel each electron spin follows a different path toward the detector due to momentum scattering, with each one having a different transit time and therefore a different precession angle, causing dephasing in the net spin accumulation. Furthermore, the spin accumulation relaxes back to its equilibrium value. The combined effect of spin dephasing and relaxation, controlled by D_s and τ_s, determine the response of the spin signal as a function of B, as shown in Fig. 2(d). This powerful technique removes the requirement to study multiple devices to extract spin parameters, as it relies on fitting the line shape of the response based only on the two fundamental parameters controlling spin transport (Jedema, Costache *et al.*, 2002). Hanle spin precession is the gold standard for the unambiguous demonstration of spin transport using a four-terminal nonlocal geometry, and it has been extensively applied to metallic (Jedema, Heersche *et al.*, 2002), semiconducting (Lou *et al.*, 2007), and graphene (Popinciuc *et al.*, 2009; Maassen *et al.*, 2012) spin channels.

Spin-transport experiments in graphene have utilized the previously described measurement techniques. The first report on spin transport demonstrated a hysteretic magnetotransport response with a 10% change in resistance by utilizing a two-terminal local geometry (Hill *et al.*, 2006). Shortly thereafter, Tombros *et al.* (2007) demonstrated room-temperature spin transport with micrometer-long spin-relaxation lengths in monolayer graphene by employing a tunnel barrier for efficient spin injection and measuring in a four-terminal nonlocal geometry. This measurement configuration then became the standard method to characterize the distinct spin-transport properties of graphene, as demonstrated by Cho, Chen, and Fuhrer (2007) and Popinciuc *et al.* (2009), who modulated spin transport in graphene via the application of *vertical* electric fields. On the other hand, the application of *lateral* electric fields has been demonstrated to produce spin drift and therefore modulate spin injection efficiencies (Józsa *et al.*, 2008; Józsa, Popinciuc *et al.*, 2009).

After the characterization of basic spin-transport properties of graphene fabricated on standard Si/SiO_2 substrates, Józsa, Maassen *et al.* (2009) examined the dominant spin-relaxation mechanism for the first time by studying the relation between momentum and spin-relaxation times in monolayer graphene. A further discussion on spin relaxation is presented in Sec. III.A. Initial devices also demonstrated the capability to achieve robust spin polarization in monolayer and multilayer graphene by demonstrating a linear dependence of nonlocal voltage on injected current up to 10 mA (Muramoto *et al.*, 2009; Shiraishi *et al.*, 2009). Such superior spin injection properties, in comparison to previous semiconductor-based devices, are a result of the transport properties of graphene and the suppression of any significant interface spin scattering, as later confirmed by the observation of identical spin-transport parameters in graphene spin valve devices measured with three- and four-terminal techniques over a wide range of temperatures (Dankert *et al.*, 2014).

B. Fundamentals of spin-orbit coupling in 2D crystals

In the solid state electrons usually move much slower than light, with a speed $v \ll c$. However, relativistic corrections are not completely negligible, representing both a major limitation to spin transport and a source of opportunities for spin injection, manipulation and detection. The leading correction in v/c is provided by the Hamiltonian

$$\mathcal{H}_{\mathrm{SO}} = \frac{1}{2m^2c^2}(\boldsymbol{\nabla} V \times \mathbf{p}) \cdot \mathbf{s}, \tag{1}$$

where m is the electron mass and $\mathbf{p}$ and $\mathbf{s} = (s_x, s_y, s_z)$ represent the linear momentum and spin operators, respectively. In a solid, V is just the crystalline potential. As a first approximation, we can consider an atomic insulator, where electrons are bound to the nuclei of the constituents of the solid by a hydrogenlike potential of the form $V(r) \propto Z/r$, with Z being the atomic number. Equation (1) can be written as $\mathcal{H}_{\mathrm{SO}} = \Delta_{\mathrm{SO}} \mathbf{L} \cdot \mathbf{s}$, where $\mathbf{L} = \mathbf{r} \times \mathbf{p}$ is the angular-momentum operator and $\Delta_{\mathrm{SO}} \propto Z/r^3$. The averaged *intra-atomic* spin-orbit coupling (SOC) is dominated by electrons close to the nucleus at distances of the order of the Bohr radius $r \sim a_B \propto Z^{-1}$, for which the nuclear field remains almost unscreened. Since the probability of finding an electron near the nucleus scales as $\sim Z^{-2}$ (Landau and Lifshitz, 1977), the intra-atomic SOC constant goes as $\Delta_{\mathrm{SO}} \propto Z^2$: the heavier the atom, the larger the relativistic effect. In fact, the fast decay of the spin-orbit interaction with the distance to the nucleus justifies a tight-binding description. For the same reasons, relativistic corrections are smaller for bands built up from higher atomic orbitals. Such Z^2 dependence of SOC in elemental 2D materials was recently demonstrated by Kurpas *et al.* (2019).

The spin quantum number reflects the way that the electronic wave function transforms under rotations. Hence, the point group of the lattice (the set of proper and improper rotations that leave the crystal structure invariant) has a strong influence on the relativistic corrections to the electronic bands. The basis of Bloch states around high-symmetry points of the

Brillouin zone must be adapted to the irreducible representations of the so-called double group (Dresselhaus, Dresselhaus, and Jorio, 2008), consisting of the original symmetry operations plus the rotation by 2π along one of the principal axes of the crystal that defines the natural spin quantization. For 2D materials, this is usually the axis perpendicular to the plane of the crystal. The bands are described in terms of the direct product $\Gamma \times D_{1/2}$, where Γ labels the irreducible representation associated with the orbital part of the wave function and $D_{1/2}$ is the spinor representation generated by Pauli matrices s_i. This group-theory approach can be simplified in practice. Typically, the strength of the spin-orbit interaction is much weaker than the energy separation between states labeled by different angular-momentum numbers. Therefore, the main orbital character of the bands does not change much, and the indices associated with the irreducible representations of the original point group are still good quantum numbers.

Improper rotations play a crucial role given the pseudovectorial nature of the spin operator. If the crystal structure possesses a complete center of inversion, then the original twofold degeneracy of the bands is preserved. Otherwise, the bands are spin split except at time-reversal symmetric points. Nevertheless, a plane of inversion always protects the perpendicular projection of the spin close to high-symmetry points. Graphene is mirror symmetric, meaning that s_z is still a good quantum number in the low-energy limit, even in the presence of relativistic interactions. Moreover, in noncentrosymmetric materials with mirror symmetry, like transition-metal dichalcogenides (TMDCs), the large spin splittings of the bands provide a strong protection of s_z against external perturbations.

Despite the small atomic number of carbon, the effect of relativistic interactions in the spectrum of its different allotropes is a subject of intensive research. The spin-orbit coupling in graphite was first analyzed in the pioneering works by Slonczewski and Weiss (1958) and Dresselhaus and Dresselhaus (1965). In Sec. II, we focus on single- and few-layer graphene allotropes and TMDCs, describing how SOC can be exploited in spintronic devices.

II. STATE OF THE ART IN GRAPHENE SPINTRONICS

A. Spin-orbit coupling in graphene

Graphene consists of a single layer of sp^2 hybridized carbon atoms (Katsnelson, 2007; Castro Neto *et al.*, 2009). In-plane $p_{x,y}$ and s orbitals participate in the strong σ bonds that keep carbon atoms covalently attached, forming a trigonal planar structure with a distance between atoms of $a = 1.42$ Å. The remaining electron occupying the p_z orbital is free to hop between neighboring sites, leading to the π bands responsible for the conductive properties. The low-energy π bands form Dirac cones at the two inequivalent corners of the hexagonal Brillouin zone. The effective Hamiltonian around these points, including relativistic corrections, reads

$$\mathcal{H} = \hbar v_F(\tau_z\sigma_x k_x + \sigma_y k_y) + \Delta_{\mathrm{KM}}\tau_z\sigma_z s_z + \Delta_{\mathrm{BR}}(\tau_z\sigma_x s_y - \sigma_y s_x), \quad (2)$$

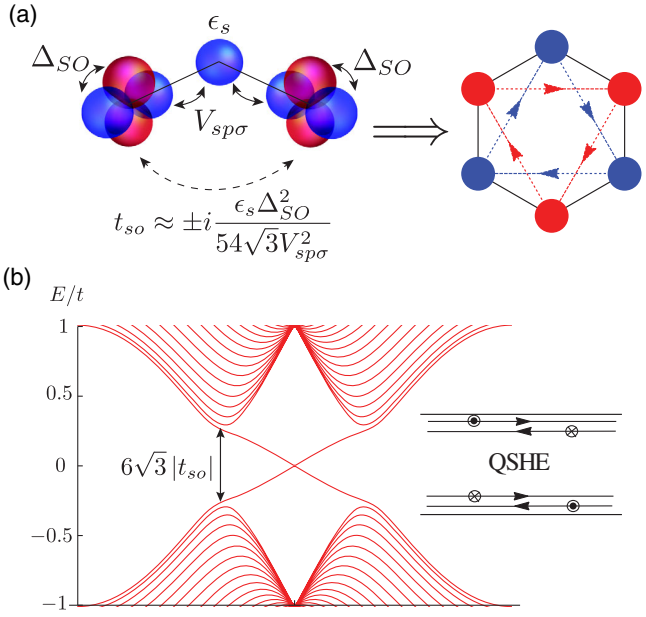

FIG. 3. (a) Spin-dependent effective hopping $t_{\mathrm{so}} = \Delta_{\mathrm{KM}}/3\sqrt{3}$ mediated by σ orbitals (in blue). The upper (lower) sign applies to spin-up (spin-down) electrons, with the hopping defined along the arrows in the right panel. (b) Electronic spectrum of a zigzag ribbon of 30 unit-cell width ($t_{\mathrm{so}} = 0.1t$, where t represents the nearest-neighbor hopping). (Inset) Sketch of the subgap counterpropagating modes localized at the edges.

where $v_F \approx c/100$ represents the Fermi velocity Dirac electrons and the operators $\sigma_{x,y,z}$ and $\tau_{x,y,z}$ are Pauli matrices acting on the sublattice and valley degrees of freedom of the wave function, respectively. The second term in Eq. (2) corresponds to the intrinsic spin-orbit coupling (Kane and Mele, 2005b). It is fully compatible with both hexagonal (C_{6v} point group) and mirror symmetries of freestanding graphene. If the latter symmetry is broken, e.g., by the presence of a substrate, then a Bychkov-Rashba coupling is also generated. The spin-orbit couplings in confined geometries were analyzed by Zarea and Sandler (2009), López-Sancho and Muñoz (2011), Lenz, Urban, and Bercioux (2013), and Santos *et al.* (2013).

The minimal microscopic model that captures spin-orbit effects should at least include both π and σ orbitals. In this model, the intrinsic SOC arises from virtual transitions into σ states mediated by the intra-atomic spin-orbit interaction, as represented in Fig. 3. Second-order perturbation theory gives (Huertas-Hernando, Guinea, and Brataas, 2006; Min *et al.*, 2006; Konschuh, Gmitra, and Fabian, 2010)

$$\Delta_{\mathrm{KM}} = \frac{\epsilon_s \Delta_{\mathrm{SO}}^2}{18 V_{sp\sigma}^2} \approx 1\ \mu\mathrm{eV}, \quad (3)$$

where $V_{sp\sigma} \approx 4.2$ eV represents the hopping between the $p_{x,y}$ and s orbitals, $\epsilon_s \approx -7.3$ eV is the energy of the latter measured with respect to the intrinsic Fermi level (Tománek and Louie, 1988), and the intra-atomic spin-orbit coupling for carbon is $\Delta_{\mathrm{SO}} \approx 7.86$ meV. This second-order effect is exceeded by the contribution from the hybridization with

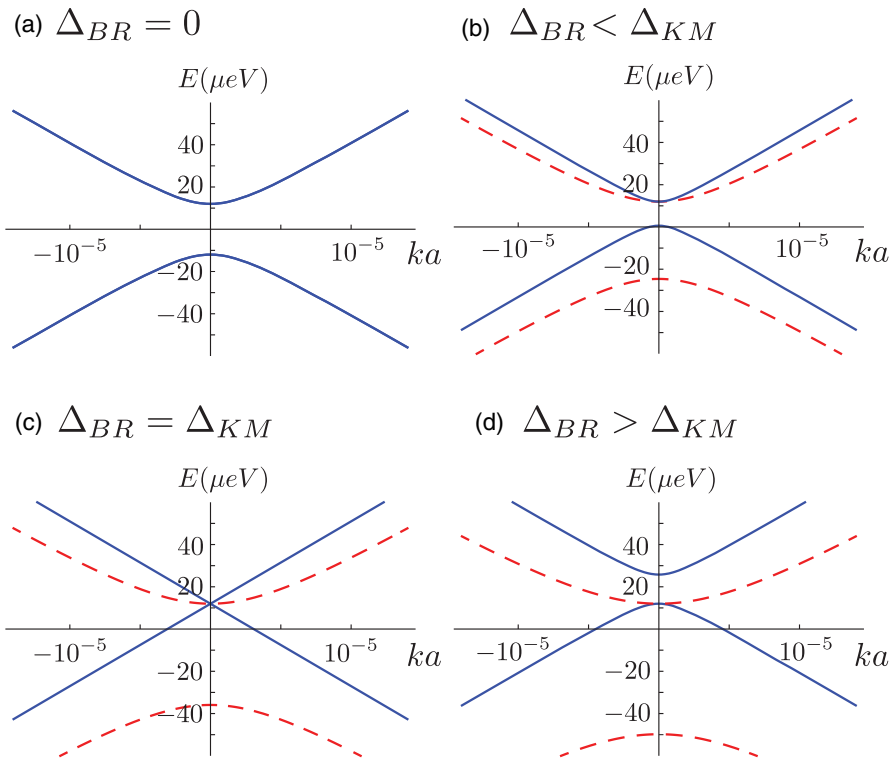

FIG. 4. Low-energy bands of graphene around the corners of the Brillouin zone (all values in μeV): (a) $\Delta_{BR} = 0$, (b) $\Delta_{BR} = 6$, (c) $\Delta_{BR} = 12$, and (d) $\Delta_{BR} = 18$ ($\Delta_{KM} = 12$ in all cases). Note that the Bychkov-Rashba coupling lifts the spin degeneracy of the bands. Solid blue and dashed red lines represent opposite helicities (the approximated spin polarization of Bloch electrons lie within the graphene plane along an axis orthogonal to their crystal momenta).

higher-energy d orbitals (Slonczewski and Weiss, 1958), leading to $\Delta_{KM} \approx 12$ μeV (Yao *et al.*, 2007; Gmitra *et al.*, 2009; Abdelouahed *et al.*, 2010; Konschuh, Gmitra, and Fabian, 2010). Electron-electron interactions (Kane and Mele, 2005b) and the coupling with flexural optical phonons can also contribute to this coupling (Ochoa *et al.*, 2012). Recent electron-spin resonance measurements gave $\Delta_{KM} \approx 21$ μeV (Sichau *et al.*, 2019).

The Bychkov-Rashba term in the second line of Eq. (2) removes the spin degeneracy of the bands and tends to close the intrinsic spin-orbit gap. As we mentioned, it is naturally present when the mirror symmetry is broken, while the planar C_{6v} symmetry is preserved. A handy example is the case of an electric field perpendicular to the graphene sample. A dipolar coupling of the form $\mathcal{H}_d = e\mathcal{E}_z \cdot z$ induces transitions between p_z and s orbitals parametrized by $\zeta \equiv \langle s|z|p_z\rangle$. The electron goes back to the π band through the intra-atomic spin-orbit interaction, flipping the spin. Perturbation theory gives (Huertas-Hernando, Guinea, and Brataas, 2006; Min *et al.*, 2006; Konschuh, Gmitra, and Fabian, 2010)

$$\Delta_{BR} = \frac{e\mathcal{E}_z \zeta \Delta_{SO}}{3V_{sp\sigma}} \approx 0.1 \text{ meV} \times \mathcal{E}_z \text{ [V/nm]}, \tag{4}$$

where $\zeta = 3a_B$ for the numerical estimation. *Ab initio* calculations lower this estimate by an order of magnitude (Gmitra *et al.*, 2009; Konschuh, Gmitra, and Fabian, 2010). Figure 4 shows the different band topologies resulting from the competition between the intrinsic and Bychkov-Rashba SOC terms.

1. hBN-Gr: Long-distance spin transport

As a result of the small intrinsic spin-orbit coupling it was expected that graphene (Gr) would exhibit a long-distance spin transport. This is evident when combining graphene with hexagonal boron nitride (hBN). Because of hBN's reduced trapped charge concentration and atomically flat surface compared to conventional SiO_2, hBN has been employed as an ideal substrate for boosting the electronic charge quality of graphene (Dean *et al.*, 2010). Recently hBN has been adapted in graphene spin valves as a substrate (Zomer *et al.*, 2012), an encapsulating layer (Guimarães *et al.*, 2014; Ingla-Aynés *et al.*, 2015; Avsar *et al.*, 2016; Gurram *et al.*, 2016), and a tunnel barrier (Yamaguchi *et al.*, 2013; Kamalakar, Dankert *et al.*, 2015; Singh *et al.*, 2016) to improve its spin-transport properties and realize new device concepts.

The first single-layer graphene-based spin valves fabricated on a hBN substrate demonstrated 20 μm distance spin transport, due to an improved spin diffusion coefficient and high electronic mobility; see Fig. 5(a) (Zomer *et al.*, 2012). Spin-relaxation times obtained in these devices exhibited comparable values to those obtained with a conventional SiO_2 substrate. This observation was attributed to spin scattering due to fabrication-related residues, and it inspired work pursuing new studies including hBN encapsulation. Improved spin-relaxation times up to 2 ns with spin-relaxation lengths exceeding 12 μm were observed in partially

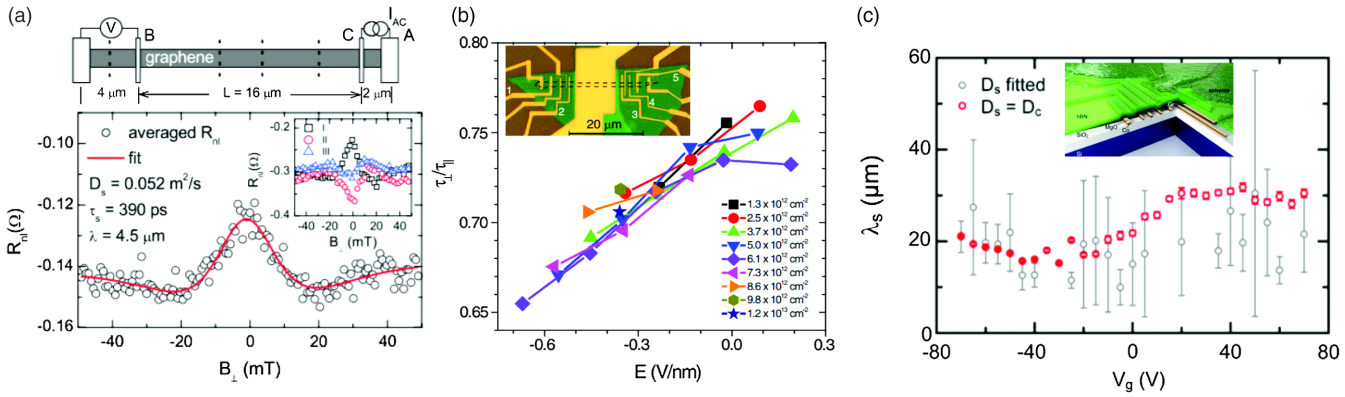

FIG. 5. High-quality heterostructures for spin transport. (a) Hanle spin precession measurement for a distance between an injector and a detector of 18 μm. From Zomer *et al.*, 2012. (b) Electric-field dependence of the ratio in- and out-of-plane injected spins at fixed carrier concentrations. (Inset) Optical picture of a completed device. From Guimarães *et al.*, 2014. (c) Back gate voltage dependence of spin-relaxation length in an inverted graphene spin valve. (Inset) Device schematics. From Drögeler *et al.*, 2016.

encapsulated graphene (Guimarães *et al.*, 2014). This device structure also allows for the study of the Rashba spin-orbit coupling and the resulting anisotropy of the spin-relaxation time for spins pointing out of plane to spins pointing in plane, and its modulation via a perpendicular electric field; see Fig. 5(b). A similar geometry was also employed for bilayer spin valve devices, leading to spin-relaxation lengths of 24 μm (Ingla-Aynés *et al.*, 2015). Avsar *et al.* (2016) performed a comparative study by discussing the effect of the substrate and polymer residues on spin transport, where the observation of similar spin-transport characteristics in nonencapsulated graphene on SiO_2 and hBN substrates suggested that spin transport in these devices was not limited by contacts, substrate phonons, or impurities.

On the other hand, observation of a fivefold enhancement in spin-relaxation times upon encapsulation, and a nonmonotonic carrier concentration dependence of spin-relaxation times, suggests that resonant scattering by unintentional magnetic impurities is the limiting source for spin scattering in graphene, consistent with a theoretical proposal (Kochan *et al.*, 2015). These studies suggest that adapting a full encapsulation process could allow one to approach graphene's intrinsic spin-transport performance. Toward this, Drögeler *et al.* (2016) developed a bottom-top approach for fabricating polymer free spin valves, where hBN encapsulated graphene was transferred on top of prefabricated Co/MgO spin electrodes. They observed record spin-relaxation times of 12 ns with spin-relaxation lengths exceeding 30 μm, despite the presence of pinholes in their MgO tunnel barriers, as shown in Fig. 5(c). These results also confirm the relevance of polymer residues for enhancing spin scattering events.

2. Bilayer and few-layer graphene

In bilayer graphene, the unit cell contains four atoms. In Bernal stacking, the low-energy bands are built up from p_z orbitals localized at opposite sublattices in different layers. The bands touch at the corners of the Brillouin zone, as in the case of graphene, but with an approximately quadratic dispersion instead (McCann and Fal'ko, 2006). This degeneracy is protected by the D_{3d} point-group symmetry of the crystal, but it can be removed by applying a perpendicular electric field (Castro *et al.*, 2007). Since the bands are quadratic, we must consider spin-orbit couplings up to linear order in crystal momentum. Within the two-band effective model, the intrinsic terms compatible with the crystallographic symmetries read (Guinea, 2010; McCann and Koshino, 2010; van Gelderen and Morais Smith, 2010; Konschuh *et al.*, 2012)

$$\mathcal{H}_{\mathrm{SO}}^{\mathrm{blg}} = \Delta_{\mathrm{KM}}\sigma_z\tau_z s_z + \Delta_{\mathrm{BR}}(k_x s_y - k_y s_x)\sigma_z. \tag{5}$$

The first term is a Kane-Mele coupling, whereas the second term adopts the form of the usual Bychkov-Rashba coupling in the 2D electron gas $k_x s_y - k_y s_x$, but with the opposite sign for electrons residing at different layers or sublattices. Notice that this term does not remove the spin degeneracy since the unit cell possesses a complete center of inversion ($D_{3d} = D_3 \times i$, where i is the inversion group). Another difference with respect to the case of single-layer graphene is that the Kane-Mele coupling is linear in the intra-atomic spin-orbit coupling due to the nonzero hybridization between π and σ orbitals localized at different layers. *Ab initio* calculations give $\Delta_{\mathrm{KM}} = 12$ μeV, $\Delta_{\mathrm{BR}} = 19$ μeV nm (Konschuh *et al.*, 2012). The low-energy bands of bilayer graphene are shown in Fig. 6.

This symmetry-based analysis can be extended to graphene multilayers with an arbitrary number of layers N (Guinea, Castro Neto, and Peres, 2006; Partoens and Peeters, 2006; Mañes, Guinea, and Vozmediano, 2007). The electronic properties of these systems depend on both N and the type of stacking. A Bernal stack with even N possesses D_{3d} symmetry. The low-energy bands can be seen as $N/2$ copies of the low-energy model of bilayer graphene. When N is odd, however, the point group of the crystal is D_{3h}. In the simplest description, an additional band with linear (Dirac) dispersion appears, but none of these degeneracies are protected by the crystallographic symmetries in this case. The low-energy spectrum of rhombohedral stacks does not depend on the parity of the number of layers. There are only two bands that touch at corners of the Brillouin zone with dispersion $|\mathbf{k}|^N$. These bands become surface states localized at the top and bottom layers in the limit $N \to \infty$. The remaining $2N-2$ bands form Dirac crossings protected by D_{3d} symmetry.

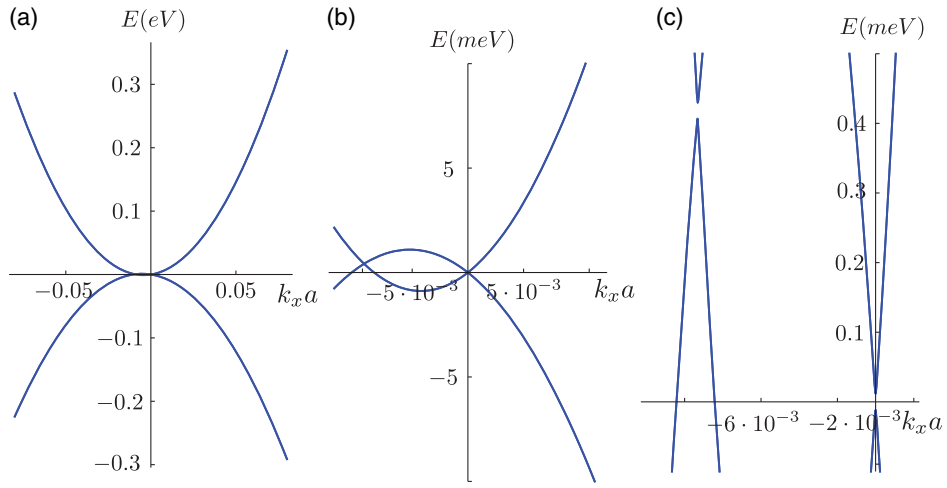

FIG. 6. Low-energy bands of bilayer graphene. (a) Parabolic dispersion of the low-energy bands around one of the inequivalent corners of the Brillouin zone. The bands localized at the carbon atoms sitting on top of each other appear at higher energies. (b) The two parabolas overlap due to the trigonal warping of the bands. The low-energy bands were obtained using density-functional theory extracted tight-binding parameters. (c) The SOC terms $\Delta_{\mathrm{KM}} = 12\ \mu\mathrm{eV}$ and $\Delta_{\mathrm{BR}} = 19\ \mu\mathrm{eV\,nm}$ (Konschuh *et al.*, 2012) lift the band crossings. Note that the bands remain spin degenerate due to inversion symmetry.

Within the lowest-energy bands of centrosymmetric stacks, only a Kane-Mele coupling is allowed by symmetry at $\mathbf{k} = 0$ (with the sublattice operators properly defined), whereas in the case of noncentrosymmetric stacks the spin-orbit coupling removes the spin degeneracy (McCann and Koshino, 2010). However, the spin polarization along the out-of-plane direction is still a good quantum number due to mirror symmetry ($D_{3h} = D_3 \times \sigma_h$, where σ_h is the mirror reflection along the basal plane).

3. The original topological insulator

Despite its weakness, the spin-orbit coupling in graphene has attracted a lot of attention in recent years due to the connection with the field of topological insulators (Hasan and Kane, 2010; Qi and Zhang, 2011). The intrinsic or Kane-Mele term removes the degeneracy at the Dirac points, opening a gap in the spectrum. Moreover, the virtual processes mediated by high energy bands resemble the pattern of complex hoppings proposed by Haldane as a model for the quantum anomalous Hall effect (Haldane, 1988). In this case, the phase $\pm\pi/2$ accumulated by the wave function is the opposite for spin up and spin down. In a finite geometry, helical modes localized at the edges of the system appear within the bulk gap, as shown in the calculation of Fig. 3. Backscattering between counterpropagating modes with opposite spin polarization is forbidden by time-reversal symmetry (Kane and Mele, 2005a; Moore and Balents, 2007; Roy, 2009). This quantum spin Hall effect (QSHE) is unobservable in practice due to the narrowness of the topological gap. Nevertheless, it has been theorized that it could be stabilized by heavy adatom deposition (Weeks *et al.*, 2011). Here we note that such an adatom-induced topological gap has not been experimentally observed yet (Chandni, Henriksen, and Eisenstein, 2015; Jia *et al.*, 2015; Wang, Cai *et al.*, 2015; Wang, Xiao *et al.*, 2015; Santos *et al.*, 2018) since such a dilute limit makes the realization of QSHE challenging (Milletarì and Ferreira, 2016).

The low SOC strength of graphene is detrimental to the implementation of graphene into many spintronics applications requiring high SOC strength such as spin FETs (Datta and Das, 1990). Moreover, it also restricts the realization of the theoretically predicted quantum spin Hall state at experimentally accessible temperatures (Kane and Mele, 2005b). All of these stimulate the development of new methods for extrinsically enhancing SOC.

B. Corrugations and resonant impurities

Corrugations naturally break the mirror symmetry of graphene, giving rise to new SOC terms. Microscopically, the origin of these new couplings is the change of relative orientation of the orbitals due to the extrinsic curvature (i.e., the bending) of the graphene sheet, which hybridizes the π and σ bands; otherwise, hopping between these orbitals would be precluded by mirror symmetry. In a low-energy continuum description, this extrinsic curvature is characterized by a second rank tensor $\mathcal{F}_{ij} \approx \partial_i \partial_j h$, with $i, j = x, y$, describing the embedding of the graphene sheet in ambient space, where the field $h(x, y)$ represents the out-of-plane displacement of carbon atoms at position (x, y). The mean curvature $\mathcal{F}_{ii} \approx \nabla^2 h$ generates a Bychkov-Rashba coupling of the form (Huertas-Hernando, Guinea, and Brataas, 2006; Jeong, Shin, and Lee, 2011; Ochoa *et al.*, 2012),

$$\mathcal{H}_{\mathrm{BR}} = g_{\mathrm{BR}} \mathcal{F}_{ii} (\tau_z \sigma_x s_y - \sigma_y s_x). \tag{6}$$

The tensorial nature of $\mathcal{F}_{ij}$ allows for additional couplings, incorporating the effect of a preferential direction of bending (Ochoa *et al.*, 2012):

$$\begin{aligned}\mathcal{H}'_{\mathrm{BR}} = {} & g_1[(\mathcal{F}_{xx} - \mathcal{F}_{yy})\tau_z s_y + 2\mathcal{F}_{xy}\tau_z s_x] \\ & + g_2[(\mathcal{F}_{xx} - \mathcal{F}_{yy})(\tau_z \sigma_x s_y + \sigma_y s_x) \\ & + 2\mathcal{F}_{xy}(\sigma_y s_y - \tau_z \sigma_x s_x)].\end{aligned} \tag{7}$$

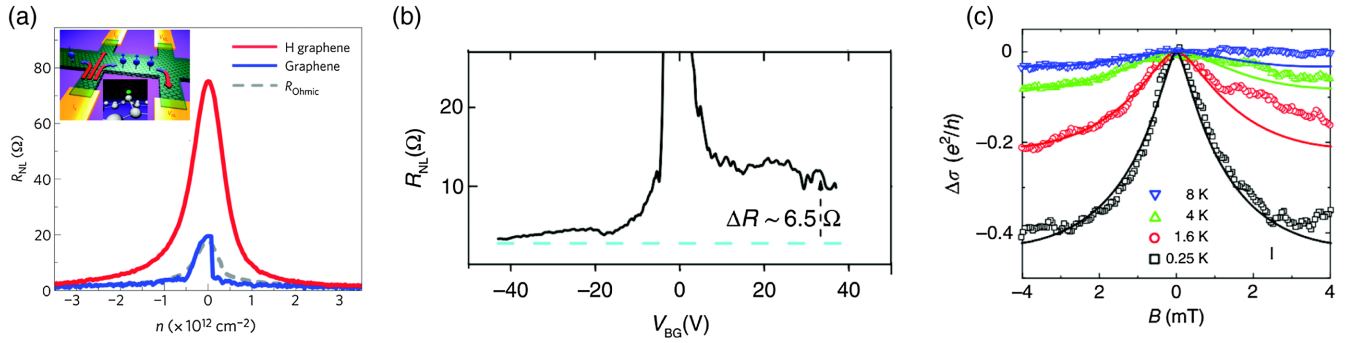

FIG. 7. Exploiting spin-orbit coupling in graphene. (a) Carrier concentration dependence of the nonlocal resistance in weakly hydrogenated ($R_{NL}^{max} \sim 80$ Ω) and pristine ($R_{NL}^{max} \sim 20$ Ω) graphene, shown as red and blue lines, respectively. The dotted gray line represents the calculated Ohmic contribution. From Balakrishnan *et al.*, 2013. (b) Back gate voltage (V_{BG}) dependence of the nonlocal resistance in graphene devices supported on WS_2. Spin precession and a sizable signal are detectable only for $V_{BG} > 0$. From Avsar *et al.*, 2014. (c) Magnetotransport measurements for graphene on a WS_2 substrate, showing a weak antilocalization effect. From Zhe Wang *et al.*, 2015.

From the previous tight-binding estimates, we have (Jeong, Shin, and Lee, 2011; Ochoa *et al.*, 2012)

$$g_{BR} = \frac{a\epsilon_s \Delta_{SO}(V_{pp\pi} + V_{pp\sigma})}{12V_{sp\sigma}^2} \approx 1.2 \text{ meV Å},$$
$$g_1 = \frac{aV_{pp\pi}\Delta_{SO}}{2(V_{pp\sigma} - V_{pp\pi})} \approx 1.5 \text{ meV Å}, \quad (8)$$

where $V_{pp\pi} \approx -2.2$ eV and $V_{pp\sigma} \approx 5.4$ eV represent the hopping between p orbitals at nearest neighbors. The second coupling in Eq. (7) appears only at second nearest neighbors, so it is usually neglected.

Since graphene is all surface, its environment sensitivity enables different ways of boosting its SOC, including functionalization, adatom decoration, and substrate engineering (Castro Neto and Guinea, 2009; Weeks *et al.*, 2011; Ma, Li, and Yang, 2012; Gmitra, Kochan, and Fabian, 2013; Ferreira *et al.*, 2014; Pachoud *et al.*, 2014; Irmer *et al.*, 2015; Soriano *et al.*, 2015). One of the first proposed strategies to enhance the SOC was the functionalization of graphene surface with hydrogen adatoms, which create a local out-of-plane, sp^3-like distortion of the surrounding bonds. This distortion hybridizes the σ states with the adjacent p_z orbitals, giving rise to an enhancement of the spin-orbit coupling (Castro Neto and Guinea, 2009),

$$\Delta \approx \tan\vartheta\sqrt{1 - 2\tan^2\vartheta}\Delta_{SO}, \quad (9)$$

where ϑ represents the angle of the distorted σ bond with respect to the graphene plane (i.e., $\vartheta = 0$ for the flat configuration). In the case of a complete sp^3 hybridization ($\vartheta = 19.5°$), we have an enhanced SOC up to $\Delta \approx 6$ meV. The symmetry is effectively reduced down to C_{3v}, so the specific couplings in the low-energy theory acquire different forms (Gmitra, Kochan, and Fabian, 2013). *Ab initio* calculations give $\Delta_{BR} \approx 0.33$ meV for the Bychkov-Rashba coupling. Notice that in this situation the bottleneck is still the weak intra-atomic spin-orbit interaction in carbon.

Balakrishnan *et al.* (2013) experimentally reported a SOC enhancement of 2.5 meV in weakly hydrogenated graphene samples; see Fig. 7(a). Such enhancement caused the observation of the spin Hall effect (SHE) at room temperature, with the spin-transport origin of the nonlocal signal confirmed by spin precession measurements. Similar results were also obtained in fluorinated graphene samples (Avsar *et al.*, 2015). Nevertheless, other studies have reported large nonlocal signals in similarly hydrogenated devices but with an absence of any magnetic field dependence in spin precession measurements (Kaverzin and van Wees, 2015) or contradiction of the expectation of a decrease in spin lifetime due to larger SOC (Wojtaszek *et al.*, 2013). The latest results suggest that the effect is sample dependent and there can be additional mechanisms involved other than spin transport, as theoretically suggested for the case of disorder in graphene (Van Tuan *et al.*, 2016). These conflicting interpretations for experiments in hydrogenated graphene call for further studies to ensure a thorough verification of the role of SOC and the presence of the SHE in this system, and to further identify any other concomitant effect leading to the nonlocal response observed.

The passivation of the p_z orbital below the adatom creates a perfect vacancy (i.e., with no reconstruction altering the coordination of the lattice). Such a defect induces the formation of a quasilocalized state, manifested as a sharp resonance in the local density of states (Pereira *et al.*, 2006; Wehling *et al.*, 2010). The enhancement of the density of states at energies close to the Dirac point favors the formation of magnetic moments due to electron-electron interactions (Palacios, Fernández-Rossier, and Brey, 2008; Yazyev, 2008), which can modify both charge and spin-transport properties. Nonperturbative calculations beyond the mean field show no signature of saturation of the susceptibility at low temperatures (Haase *et al.*, 2011), suggesting a ferromagnetic coupling between the quasilocalized magnetic moment and the itinerant spins. Nevertheless, experiments have thus far demonstrated a paramagnetic response (McCreary *et al.*, 2012; Nair *et al.*, 2012).

Another direction to enhance the weak SOC of graphene is the decoration of its surface with heavy metallic adatoms (Weeks *et al.*, 2011; Hu *et al.*, 2012; Ma, Li, and Yang, 2012;

Ferreira *et al.*, 2014; Pachoud *et al.*, 2014; Brey, 2015; Cysne, Ferreira, and Rappoport, 2018). In this approach, the sp^2 bond property of graphene is preserved; the SOC is locally enhanced due to tunneling of electrons from graphene to adatoms and back. Marchenko *et al.* (2012) observed a giant spin-orbit splitting of ≈0.1 eV in Au intercalated graphene samples. The photoelectron spectroscopy measurements revealed that hybridization with Au $5d$ states is the source of spin-orbit splitting. Large spin-orbit fields were also achieved in Pb intercalated graphene on an Ir substrate (Calleja *et al.*, 2015). Balakrishnan *et al.* (2014) reported the spin Hall effect at room temperature in chemical vapor deposition (CVD) grown graphene devices, attributed to unavoidable residual Cu adatom clusters, with a SOC of ≈20 meV. However, there are experimental controversies over nonlocal measurements in adatom decorated samples as well. For example, other groups also reported large nonlocal signals in Au and Ir decorated samples, but they did not observe any magnetic field dependence (Wang, Cai *et al.*, 2015). Further work is therefore needed to address the possible role of valley currents or of variations in adatom cluster sizes.

C. Transition-metal dichalcogenides and graphene

The family of atomically thin 2D crystals goes beyond the allotropes of carbon and already includes materials like phosphorene (Xia, Wang, and Jia, 2014), graphane C_2H_2 (Elias *et al.*, 2009), and monolayers of hBN (Watanabe, Taniguchi, and Kanda, 2004), among others (Geim and Grigorieva, 2013). Silicene (Fleurence *et al.*, 2012; Vogt *et al.*, 2012), a single layer of silicon atoms forming an sp^3-like honeycomb lattice, has attracted much attention due to its resemblance to graphene. The spin-orbit coupling within the π bands reduces to Eq. (5) as imposed by D_{3d} point-group symmetry. The Kane-Mele coupling is much larger than in graphene, $\Delta_{\mathrm{KM}} \sim 1.5$ meV, due to its buckled structure. For the same reason, the band topology can be controlled by applying a perpendicular electric field (Drummond, Zolyomi, and Fal'ko, 2012; Ezawa, 2012).

The most appealing materials regarding spintronics applications are probably monolayers of TMDCs (Wang *et al.*, 2012). Bulk compounds are composed of X-M-X layers (with X representing the chalcogen atoms and M representing the transition metal) stacked on top of each other and coupled by weak van der Waals forces. They show different polytypes that vary in stacking and atom coordination (Wang *et al.*, 2012). Like graphite these materials can be exfoliated down to a single layer (Gordon *et al.*, 2002). Semiconducting materials include molybdenum disulfide (MoS_2), tungsten disulfide (WS_2), molybdenum diselenide ($MoSe_2$), and tungsten diselenide (WSe_2) (Mak *et al.*, 2010).

The point group of the monolayer crystal is D_{3h}. The lattice consists in a triangular Bravais lattice with two X atoms and one M atom per unit cell. As in the case of graphene, the Fermi level lies around the two inequivalent corners of the hexagonal Brillouin zone. However, the dispersion and orbital character of the conduction and valence bands are completely different. The large crystal fields associated with the different atomic species prevent accidental degeneracies, so the bands remain gapped with approximately quadratic dispersion (Cappelluti *et al.*, 2013; Rostami, Moghaddam, and Asgari, 2013). The spin-orbit interaction splits the spin degeneracy of the bands,

$$\mathcal{H}_{\mathrm{SO}}^{\mathrm{tmd}} = \lambda_c \frac{1+\sigma_z}{2}\tau_z s_z + \lambda_v \frac{1-\sigma_z}{2}\tau_z s_z. \tag{10}$$

TABLE I. Band spin splittings in monolayers of transition-metal dichalcogenides. Values from Zhu, Cheng, and Schwingenschlogl (2011), Feng *et al.* (2012), and Kormanyos *et al.* (2013).

Material	λ (meV)
MoS_2 (conduction band)	3
MoS_2 (valence band)	140
WS_2 (valence band)	430
$MoSe_2$ (valence band)	180
WSe_2 (valence band)	460

The magnitudes of the splittings in conduction and valence bands are significantly different due to their distinct orbital character, dominated by d orbitals from the transition metal in both cases. A complete tight-binding model can be found in Roldán *et al.* (2014). Values extracted from *ab initio* calculations (Zhu, Cheng, and Schwingenschlogl, 2011; Feng *et al.*, 2012; Kormanyos *et al.*, 2013) are summarized in Table I. Notice that the splittings of the bands have opposite signs at each valley, as imposed by time-reversal symmetry. This spin-valley coupling (Xiao *et al.*, 2012) enables the optical control of valley populations (Cao *et al.*, 2012; Mak *et al.*, 2012; Zeng *et al.*, 2012). As discussed in Sec. II.D, this property allows generation of spin-polarized charge carriers without the need for a ferromagnetic spin injector.

Graphene placed on top of a TMDC forms an appealing heterostructure from the point of view of spintronics. The Dirac cone lies within the gap of the transition-metal dichalcogenide, so the low-energy π bands preserve their identity while acquiring a large spin-orbit coupling by their proximity to the heavy atoms in the second layer (Kaloni *et al.*, 2014; Gmitra *et al.*, 2016; Wang *et al.*, 2016). The dispersion is well described by (Gmitra and Fabian, 2015; Alsharari, Asmar, and Ulloa, 2016; Kochan, Irmer, and Fabian, 2017)

$$\begin{aligned}\mathcal{H}_{\mathrm{gr/tmd}} = {} & \hbar v_F(\tau_z\sigma_x k_x + \sigma_y k_y) + \Delta_{\mathrm{st}}\sigma_z + \Delta_{\mathrm{KM}}\tau_z\sigma_z s_z \\ & + \Delta_{\mathrm{BR}}(\tau_z\sigma_x s_y - \sigma_y s_x) + \lambda\tau_z s_z. \end{aligned} \tag{11}$$

A comparison to Eq. (2) reveals two new terms in this Hamiltonian: the staggered potential Δ_{st}, which opens a trivial gap in the spectrum, and the last term in the second line of Eq. (11), which removes the spin degeneracy of the bands. Both terms reflect the fact that the symmetry of graphene is effectively reduced down to C_{3v} due to the interaction with the underlying TMDC system. The model can be generalized to describe heterostructures with bilayer graphene, for which the induced spin-orbit coupling can be tuned by applying a perpendicular electric field (Gmitra and Fabian, 2017; Khoo, Morpurgo, and Levitov, 2017). Such tunability makes bilayer graphene on WSe_2 an efficient field-effect spin-orbit valve (Gmitra and Fabian, 2017).

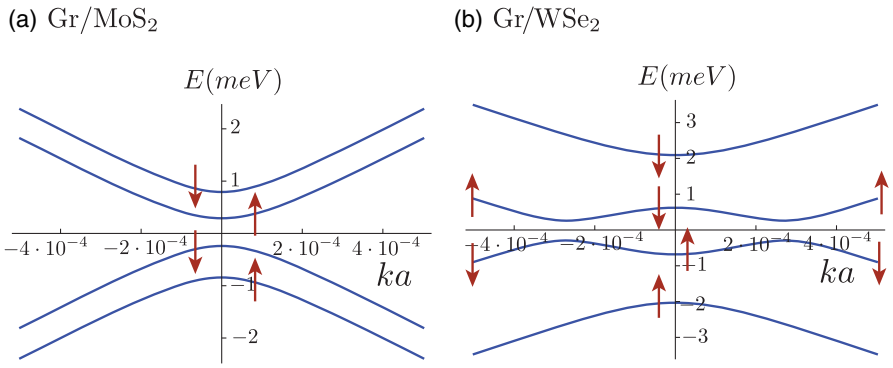

FIG. 8. Low-energy bands of graphene on (a) MoS_2 and (b) WSe_2 deduced from the Hamiltonian in Eq. (11). The values of the parameters correspond to (Gmitra *et al.*, 2016) (a) $\Delta_{st} = 0.52$, $\Delta_{KM} = -0.025$, $\Delta_{BR} = 0.13$, $\lambda = -0.255$, and (b) $\Delta_{st} = 0.54$, $\Delta_{KM} = -0.03$, $\Delta_{BR} = 0.56$, $\lambda = -1.19$ (all values are in meV). The arrows indicate the (approximate) spin polarization of the bands, which is the opposite at different valleys.

Two distinctive band dispersions arise from this model, as represented in Fig. 8. In the first case [Fig. 8(a)] the staggered potential dominates over the induced spin-orbit coupling, whereas in the second case [Fig. 8(b)] the spin-orbit coupling produces a band inversion. This second case is expected to occur for the heaviest atomic species in the second layer (namely, W and Se). The band inversion resembles a time-reversal symmetric version of the quantum anomalous Hall effect proposed in graphene interacting with a heavy magnet (Qiao *et al.*, 2010, 2014), where the term parametrized by λ can be interpreted as a valley-dependent exchange coupling. However, this band inversion does not correspond to a topological state like in the idealized case of pristine graphene (Fig. 3): in general, two pairs (instead of one pair) of subgap helical modes connected by time-reversal symmetry appear at the boundaries of the system (Yang *et al.*, 2016). Backscattering between states belonging to different Kramers doublets (in a zigzag ribbon, one pair around the projected K and K' points and the other at M) is precluded only by crystalline symmetries, which are removed by generic disorder. Moreover, the edges states are completely absent in armchair ribbons.

The approaches for enhancing SOC in graphene previously discussed in Sec. II.B regarding functionalization (Balakrishnan *et al.*, 2013; Avsar *et al.*, 2015) and adatom decoration (Balakrishnan *et al.*, 2014) had the downside of reducing the electronic quality of graphene. On the other hand, creating a van der Waals interface between graphene and a TMDC can enhance the SOC of the former while simultaneously preserving its high electronic mobility (Tan *et al.*, 2014). Toward this, Avsar *et al.* (2014) reported a 3 order of magnitude enhancement of SOC strength by bringing graphene into proximity with WS_2. The resulting large SOC strength of up to 17.6 meV led to the observation of SHE or inverse SHE (ISHE) for transport in the electron regime, attributed to sulfur-based in-gap defect states; see Fig. 7(b). The large spin-orbit coupling in sulfur vacancies in monolayer WS_2 has recently been confirmed by detailed scanning probe microscopy studies (Schuler *et al.*, 2018).

The relative strength of the induced spin-orbit couplings can be extracted from magnetotransport experiments. Zhe Wang *et al.* (2015) demonstrated pure interface-induced SOC enhancement by performing weak antilocalization measurements; see Fig. 7(c). The last two terms in Eq. (11) possess different symmetry with respect to mirror reflection, which provides different signatures in the quantum-interference correction to the conductivity. In the absence of intervalley scattering, the magnetoconductance is given by (McCann and Fal'ko, 2012)

$$\Delta G = -\frac{e^2}{2\pi h}\left[F\left(\frac{B}{B_\phi}\right) - F\left(\frac{B}{B_\phi + 2B_{\mathrm{asy}}}\right) - 2F\left(\frac{B}{B_\phi + B_{\mathrm{sym}} + B_{\mathrm{asy}}}\right)\right], \tag{12}$$

where $F(z) = \log z + \Psi(1/2 + 1/z)$, $\Psi(x)$ is the digamma function, and $B_i \equiv \hbar/(4e\ell_i^2)$. Here $\ell_{\mathrm{sym(asy)}}$ correspond to the spin diffusion lengths limited by mirror symmetric (asymmetric) spin-orbit terms, whereas ℓ_ϕ represents the phase-coherence length limited by inelastic scattering (phonons or electron-electron interactions). While spin dephasing induced by mirror asymmetric terms (i.e., the Bychkov-Rashba coupling) should be manifested as a weak antilocalization effect at low temperatures and fields, the mirror symmetric terms (i.e., the spin-valley locking term λ) introduces an effective saturation of the decoherence times, leading to a suppression of the magnetoconductance at the lowest fields ($B < B_{\mathrm{sym}}$). A similar crossover is expected in TMDC monolayers (Ochoa *et al.*, 2014). In hybrid graphene-TMDC systems, a weak antilocalization behavior is systematically reported, as discussed previously, in a wide range of carrier concentrations (Zhe Wang *et al.*, 2015; Wang *et al.*, 2016; Yang *et al.*, 2016, 2017), suggesting a dominance of mirror asymmetric terms. Extracting the strength of the couplings requires the knowledge of the underlying spin-relaxation mechanism, which is the subject of Sec. III.A. Alternatively, for quantizing fields one can trace the effect of different SOC couplings in the sequence of Landau levels (Cysne *et al.*, 2018; Khoo and Levitov, 2018). Overall, the observation of similar results with different dichalcogenides indicates the robust and strong

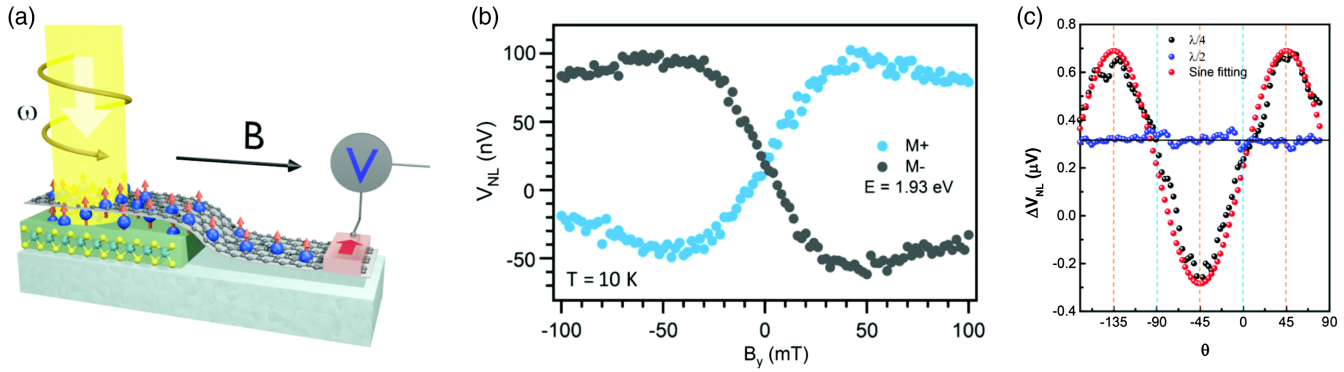

FIG. 9. Alternative spintronics in graphene and other 2D materials. (a) Schematics of optical spin injection in graphene (gray, top layer) by utilizing a monolayer transition-metal dichalcogenide (green, bottom layer) and excitation with circularly polarized light. From Gmitra and Fabian, 2015. (b) Hanle spin precession curves for different detector magnetization directions in a graphene-MoS_2 device. The detector electrode with in-plane magnetization direction $M+$ ($M-$) measures positive (negative) signal above (below) zero field. From Luo *et al.* (2017). (c) Incident angle dependence of optically generated nonlocal signal under quarter and half wave modulations in a graphene/WSe_2 device. In sharp contrast to the quarter wave modulation case, the nonlocal signal for half wave modulation shows extremely weak dependence on θ. From Avsar, Unuchek *et al.*, 2017.

nature of proximity-induced SOC enhancement in graphene-TMDC heterostructures.

The possible topological phases created by proximity-induced SOC are largely enriched in graphene multilayers. In that case, the band topologies crucially depend on the parity number of layers and stacking order, and they can be tuned by displacement field (Zaletel and Khoo, 2019). The fundamental observation is that layer-resolved spin-valley couplings enter as an effective Kane-Mele mass in the low-energy chiral bands of rhombohedral stacks due to the equivalence between layer and sublattice projections. In bilayer-graphene–TMDC heterostructures, recent electronic compressibility measurements have revealed a SOC-induced band inversion compatible with $\lambda = 1.7$ meV (Island *et al.*, 2019), which is close to theoretical estimations. In these devices, magnetotransport data suggest the existence of helical edge channels. Although backscattering (similar to the monolayer case discussed previously) is not forbidden by time-reversal symmetry, these states are expected to be more resilient against mirror asymmetric (Rashba-like) couplings thanks to interlayer coupling.

D. Graphene-TMDC optospintronics

Nondestructive optical spin injection into graphene has the potential to overcome limitations inherent to electrical spin injection methods while enabling new opto-spintronic functionalities. The weak optical absorption and weak intrinsic SOC strength of graphene prevents such a direct optical spin injection (Inglot *et al.*, 2014). Silicon also poses a similar challenge toward spin injection due to its low SOC strength. Combining Si with a direct band gap semiconductor has been proposed to overcome this challenge (Žutić, Fabian, and Erwin, 2006). In this regard, Gmitra and Fabian (2015) proposed the use of proximity-induced SOC as way to enable direct optical spin injection. Here graphene is partially covered by a monolayer transition-metal dichalcogenide crystal, as shown in Fig. 9(a). Excitation with circularly polarized light on the TMDC-covered graphene area generates spin-polarized charge carriers in the TMDC monolayer, as a result of spin-valley coupling and the valley-selective absorption. These carriers diffuse into the adjacent graphene layer and are finally detected electrically using ferromagnetic contacts in a nonlocal geometry. These nondestructive optical spin injection schemes were recently experimentally realized independently by two groups. Luo *et al.* (2017) utilized monolayer MoS_2 to inject spin current into multilayer graphene at room temperature. They utilized Hanle spin precession measurements to confirm optical spin injection, spin transport, and electrical detection; see Fig. 9(b). Avsar, Unuchek *et al.* (2017) utilized monolayer WSe_2 to inject spin current into monolayer graphene, where the generated nonlocal spin signal was electrically detected by utilizing hBN as a tunnel barrier. The spin-coupled valley-selective origin of the signal was confirmed by prudently studying the dependences of the nonlocal spin signal on modulations of the incident light intensity and polarization; see Fig. 9(c). In future experiments, it will be relevant to determine the types of charge carriers diffusing into graphene, as well as to experimentally demonstrate the optical detection of the generated spin signal, free from any contact-related spin scattering at FM/NM interfaces.

III. CURRENT CHALLENGES AND A WAY FORWARD

A. What is the dominant spin-relaxation mechanism?

The polarization of a spin current in a metal or semiconductor device decays during the propagation of the spin carriers. Defining a characteristic time of decay in a rigorous way is a difficult task, though. This is usually introduced within the framework of the Bloch-Torrey equations (Bloch, 1946; Torrey, 1956) describing the macroscopic dynamics of the spin density in the material. Related phenomenological models can be used to fit the experimental data and extract characteristic times of spin relaxation. However, a theoretical evaluation requires more sophisticated models for the microscopic spin dynamics. Once this is determined, a quantum kinetic equation for the spin-ensemble dynamics can be derived (Mishchenko,

Shytov, and Halperin, 2004). Microscopic expressions for the relaxation rates can be obtained in the limit of long wavelengths, in which the variations of the density matrix are smooth on the scale of the characteristic length of the problem, e.g., the mean free path ℓ in the diffusive regime (Burkov, Núñez, and MacDonald, 2004). This procedure is usually simplified by a semiclassical treatment based on the spin- Boltzmann equation. This approach has been applied to the study of spin relaxation in a single layer (Zhou and Wu, 2010; Dugaev, Sherman, and Barnás, 2011; Zhang and Wu, 2011, 2012) and bilayer (Diez and Burkard, 2012) graphene, and more recently in transition-metal dichalcogenides (Wang and Wu, 2014a, 2014b).

Four main mechanisms of spin relaxation are usually discussed for metals and semiconductors (Žutić, Fabian, and Das Sarma, 2004): the Elliot-Yafet (Elliot, 1954; Yafet, 1963), D'yakonov-Perel' (D'yakonov and Perel', 1971; D'yakonov, 2008), Bir-Aronov-Pikus (Bir, Aronov, and Pikus, 1975), and hyperfine-interaction mechanisms (D'yakonov and Perel', 1973). The last two are usually disregarded in the context of graphene. On the one hand, the natural abundance of carbon isotopes with nuclear magnetic moments is extremely low; in addition, the nuclear fields acting on the spin of itinerant electrons averages out in the diffusive limit, so this contribution can be safely neglected in the experimental situations that we discuss here (Wojtaszek *et al.*, 2014). On the other hand, the Bir-Aronov-Pikus mechanism accounts for electron spin-flip processes mediated by the electron-hole exchange interaction, and therefore it is relevant only in heavily p-doped semiconductors.

The Elliot-Yafet (EY) mechanism takes into account the change in spin polarization of a Bloch electron due to scattering off phonons or impurities. It is characterized by a linear relation between the spin and the quasimomentum relaxation times $\tau_s = \alpha\tau_p$, where α can be interpreted as the spin-flip probability during a scattering event. This relation can be deduced by treating the spin-orbit interaction perturbatively and holds experimentally for most conventional metals (i.e., systems with a well-defined Fermi surface). In doped graphene, the EY mechanism is dominated by interband transitions and the Elliot relation depends explicitly on the carrier concentration (Huertas-Hernando, Guinea, and Brataas, 2009; Ochoa, Castro Neto, and Guinea, 2012),

$$\frac{1}{\tau_s} \approx \left(\frac{\Delta}{\epsilon_F}\right)^2 \tau_p^{-1}. \tag{13}$$

Here Δ represents the strength of the spin-orbit interaction within the π bands and $\epsilon_F = \hbar v_F\sqrt{\pi n}$ is the Fermi energy with respect to the Dirac point, where n represents the carrier concentration. For typical values of these parameters, $\Delta \approx 10\ \mu$eV, $n = 10^{12}$ cm^{-2}, and $\tau_p = 10$ fs, the spin-relaxation times due to the EY mechanism are of the order of $\tau_s \approx 10\ \mu$s, ≈4 orders of magnitude longer than the relaxation times reported in Hanle precession experiments.

The D'yakonov-Perel' (DP) mechanism accounts for the spin dephasing between scattering events. As discussed, the doubly degeneracy of the bands is lifted in noncentrosymmetric crystals, and the spin-orbit coupling can be interpreted as an effective Zeeman field that makes the electron spin precess in the Bloch sphere. The axis of precession depends on the direction of motion of the electron, and therefore scattering randomizes the process. This is an example of motional narrowing, characterized by the inverse relation between the spin and the quasimomentum relaxation times (Fabian *et al.*, 2007),

$$\frac{1}{\tau_s} \approx \left(\frac{\Delta_{\mathrm{BR}}}{\hbar}\right)^2 \tau_p. \tag{14}$$

The term in parentheses must be interpreted as the effective Larmor frequency associated with a Bychkov-Rashba coupling generated by the interaction with the substrate (Ertler *et al.*, 2009). Realistic estimates lead to $\tau_s \approx 1\ \mu$s, again much longer than the relaxation times reported in Hanle precession. This discrepancy in several orders of magnitude along with the shortcomings of Eqs. (13) and (14) to reproduce the intricate behavior of τ_s as a function of doping or temperature (particularly in the case of bilayer graphene) has provoked tremendous activity in recent years.

1. Intrinsic relaxation sources

As discussed, out-of-plane displacements enhance the strength of the spin-orbit coupling within the π bands due to hybridizations with higher σ states. Therefore, flexural phonons (the quanta of these vibrations) represent an unavoidable source of spin decoherence in clean, freestanding graphene. In fact, flexural phonons constitute the leading scattering mechanism in suspended samples at temperatures $T \gtrsim 10$ K, limiting the electron mobilities to a few $m^2/V\,s$ (Castro *et al.*, 2010). Their contribution to spin relaxation can be evaluated from the couplings in Eqs. (6) and (7) leading to (Fratini *et al.*, 2013; Vicent, Ochoa, and Guinea, 2017)

$$\frac{1}{\tau_s} = \frac{\tilde{g}^2 k_F}{2\hbar^2 v_F}\frac{k_B T}{\kappa}\left(\frac{2k_F}{q_c}\right)^{2\nu}, \tag{15}$$

where $\tilde{g}^2 \equiv g_{\mathrm{BR}}^2 + g_1^2/4 + g_2^2$ is the effective spin-phonon coupling. Here $\nu = 0,\ 1$ corresponds to the freestanding regime ($q_c \ll 2k_F$, where k_F is the Fermi momentum of carriers and q_c represents an infrared cutoff of the harmonic phonon dispersion) and samples under tension, respectively. In the former case, the dispersion relation of flexural phonons is quadratic $\omega_{\mathbf{q}} = \sqrt{\kappa/\rho}|\mathbf{q}|^2$, where $\kappa \approx 1$ eV (Kudin, Scuseria, and Yakobson, 2001) is the bending rigidity. At momenta $|\mathbf{q}| < q_c$, the dispersion relation is effectively linearized due to anharmonic effects (Zakharchenko *et al.*, 2010) or applied tensions, altering the dependence on the Fermi wave vector $k_F = \sqrt{\pi n}$ when the strain exceeds $\bar{u} \approx 4\pi n\kappa/K$, with $K \approx 21$ eV Å^{-2} being the two-dimensional bulk modulus (Lee *et al.*, 2008). In freestanding graphene, the spin-relaxation times are of the order of hundreds of nanoseconds at room temperature, rapidly decreasing when tension is applied. Note also that the spin-relaxation rate in Eq. (15) grows linearly with the temperature, in contrast to momentum scattering, dominated by two-phonon processes. This leads to a distinctive T^2 dependence in the mobilities of suspended

samples (Castro *et al.*, 2010), so the spin-relaxation times are expected to deviate from Eq. (13) in the clean limit.

In supported samples, graphene remains pinned to the substrate and the contribution from flexural phonons is strongly suppressed. Nevertheless, the interaction with the substrate enhances the spin-orbit coupling and induces spin relaxation (Ertler *et al.*, 2009). In addition, supported graphene sheets present static corrugations with characteristic heights of $h_0 \approx 0.3$ nm (Locatelli *et al.*, 2010), which in the simplest approximation creates a nonuniform Bychkov-Rashba coupling. In the diffusive limit, we end up with two different regimes of spin relaxation arising from the competition between the two relevant length scales in the problem, the mean free path ℓ and the lateral size of the ripples $\mathcal{L}$. In the scattering-dominated regime $\ell \ll \mathcal{L}$, spin decoherence is limited by the conventional motional narrowing. Between scattering events, the electron spin precesses an angle δ, which can be estimated from the Larmor frequency $\Delta_{\mathrm{BR}}/\hbar$, where $\Delta_{\mathrm{BR}} \approx g_{\mathrm{BR}} h_0/\mathcal{L}^2$ is the average strength of the corrugation-induced spin-orbit coupling. After N collisions and assuming that the process is Markovian, the precession angle is about $\delta(N) \sim (\Delta_{\mathrm{BR}}/\hbar)\tau_p\sqrt{N}$. The spin-relaxation time may be defined as the time after which the precession angle is $\delta(N_s = \tau_s/\tau_p) \sim 1$, from which we deduce the DP relation in Eq. (14). On the contrary, if $\ell \gg \mathcal{L}$ the randomization process is dominated by the spatial fluctuations in the strength of the spin-orbit coupling (Dugaev, Sherman, and Barnás, 2011). Within a region of characteristic size $\mathcal{L}$, we have $\delta \sim \mathcal{L}\Delta_{\mathrm{BR}}/\hbar v_F$, and after a time t we end up with $\delta(t) \sim \sqrt{t\mathcal{L}/v_F}\Delta_{\mathrm{BR}}/\hbar$. From the previous arguments, we obtain $\tau_s \sim (\Delta_{\mathrm{BR}}/\hbar)^2\mathcal{L}/v_F$ in that case. Typical ripples in graphene extend over $\mathcal{L} = 10$–50 nm ($\ll \ell$), so we expect the spin-relaxation times to be determined by geometrical parameters only and not by the scattering times. Diffusion-barrier-induced corrugations in epitaxial growth fronts are also characterized by a constant periodicity, systematically observed in CVD samples. Experimentally, however, corrugations do not seem to play an important role in spin transport (Avsar *et al.*, 2011), manifesting basically the same features in CVD graphene as in exfoliated samples.

Thus far it appears that neither of these mechanisms rely on the characteristic Dirac spectrum of low-energy graphene quasiparticles. Numerical studies suggest that the entangled dynamics of the spin and pseudospin degree of freedom (the latter associated with the projection of the wave function at different sublattices) leads to fast spin relaxation at energies close to the Dirac point (Tuan *et al.*, 2014). This mechanism qualitatively explains the dependence of τ_s on the carrier concentrations, which cannot be attributed to the usual EY and DP relations, Eqs. (13) and (14). Experimental validation of the roles of spin and pseudospin degrees of freedom (Roche and Valenzuela, 2014) and of their relative contributions compared to other sources (e.g., extrinsic; see next section) is crucial to understand the nature of spin relaxation, which is one of the fundamental long-standing puzzles standing in the way of full maturity of the field of graphene spintronics.

2. Extrinsic sources: Impurities

The observed small spin-relaxation times in graphene could have an extrinsic origin. Kochan, Gmitra, and Fabian (2014) proposed that local magnetic moments localized on resonant impurities behave as spin hot spots and cause high spin-relaxation rates. Based on this mechanism, electrons tend to stay around the impurity (Huang, Chong, and Cazalilla, 2016) and spin flip is due to the exchange interaction with the magnetic moment on the impurity. Quantitative agreement with experiment on spin-relaxation times was achieved even for an extremely low concentration of local moments. It was also predicted that spin-relaxation times in single-layer and bilayer graphene have opposite dependences on carrier concentration (Kochan *et al.*, 2015). This opposite dependence was experimentally verified by carrier concentration–dependent spin-transport measurements in hBN-encapsulated graphene (Avsar *et al.*, 2016). The last work also probed a sharp increase of spin-relaxation time in bilayer graphene at high carrier densities, which similarly can be explained with the resonant scattering theory. The source of resonant magnetic scatterers is hypothesized to be polymer residue from the device fabrication.

Moreover, Eq. (13) is not consistent with the approximately linear scaling between τ_s and the diffusion constant at different gate voltages observed in many experiments (Józsa, Maassen *et al.*, 2009; Avsar *et al.*, 2011; Han and Kawakami, 2011; Yang *et al.*, 2011). The experiments by Jo *et al.* (2011) are a notable exception for which the relation in Eq. (13) seems to hold. The large spin-orbit coupling required to fit the data ($\Delta \approx 10$ meV, close to the intra-atomic coupling in carbon) suggests that covalently attached adatoms instead of charged impurities dominate spin transport in that case. A unifying theory has been provided by Zhang and Wu (2012), suggesting that both the EY and D'yakonov-Perel' mechanisms cohabit in general, with their relative strength being dictated by ambient conditions. Recently Kochan and Fabian (2019) investigated spin relaxation in graphene in proximity to an s-wave superconductor in the presence of resonant impurities, which allows one to compare the relaxation due to magnetic and spin-orbit impurities. This theoretical work calls for experimental verification in systems such as superconductivity proximitized graphene (Žutić *et al.*, 2019).

B. Advances in spin injection contacts

A tunnel barrier is a key element of graphene spin valve devices to alleviate the conductivity mismatch problem, which dictates that the spin injection efficiency decreases if the contact resistance is too low (Rashba, 2000). To achieve a spin-dependent tunnel barrier, the pioneering work of Tombros *et al.* (2007) utilized an electron beam evaporator to grow an ≈0.6 nm thick Al layer on graphene under high vacuum conditions, followed by its oxidation in a 100 mbar O_2 pressure. These initial devices and the follow-up work using MgO barriers typically exhibit spin injection efficiencies of ≈5% (Wang *et al.*, 2008; Yang *et al.*, 2011). On the other hand, Dlubak *et al.* (2010) and B. Dlubak *et al.* (2012) characterized sputter deposited Al_2O_3 and MgO layers. Sputter deposition is a standard method to grow barriers in tunnel magnetoresistance (TMR) structures, and resulted in nearly pinhole free ≈1 nm thick Al_2O_3 barrier on graphene. Nevertheless, this method destroyed the structural quality of graphene sheets, as evidenced by the observation of strong

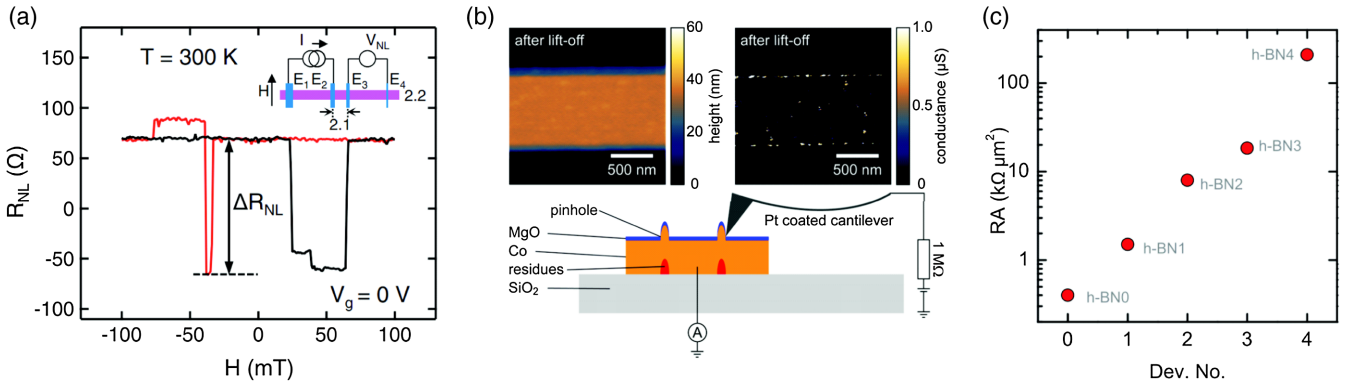

FIG. 10. Advances in spin injection contacts. (a) Large nonlocal spin valve signal of single-layer graphene measured at room temperature. The tunnel barrier is a TiO_2 seeded MgO layer. From Han *et al.*, 2010. (b) Schematic illustration of the conductance force microscopy setup together with the height and conductance mapping of one of the MgO/Co electrodes. The are bright dots in the conductance scan, representing the location of pinholes having conductance of 1 μS. From Drögeler *et al.*, 2016. (c) Tunneling characteristics of hBN barriers measured from several graphene spin valve devices. From Kamalakar, Dankert *et al.*, 2015.

Raman peaks associated with the defects (B. Dlubak *et al.*, 2012). Spin valves prepared with Al_2O_3 barriers grown by atomic-layer deposition similarly achieved spin injection efficiencies of ≈5% (Yamaguchi *et al.*, 2012). Furthermore, Komatsu *et al.* (2014) oxidized thermally evaporated yttrium barriers in air to form 1 nm thick yttrium oxide tunnel barriers and achieving spin injection efficiency of 15%.

Although most spin injection barriers dominated by pinholes, e.g., using MgO or Al_2O_3, allowed spin injection and detection, the extracted short spin-relaxation lengths were associated with contact-induced spin scattering. Therefore, a significant effort has been given to improve the quality of these barriers. In this regard, Han *et al.* (2010) achieved tunnel spin contacts with polarization of up to 30% by adding a thin Ti seed layer at the interface of MgO and graphene. Spin signals up to 130 Ω were observed, 2 orders of magnitude higher than the typical values achieved by using transparent contacts; see Fig. 10(a). Consequently, these devices exhibited improved spin-relaxation times of up to 0.5 ns. Furthermore, Drögeler *et al.* (2016) increased spin-relaxation times up to 12 ns by utilizing MgO barriers evaporated on Cobalt electrodes, just before the mechanical transfer of a encapsulating graphene-hBN heterostructure. Curiously, contact resistance measurements and scanning force microscopy show the presence of pinholes in the MgO barrier; see Fig. 10(b).

Two-dimensional crystals such as functionalized graphene or hBN are expected to act as ideal ultrathin tunnel barriers without pinholes. Prior to spin-transport measurements, the potential of hBN as a tunnel barrier was demonstrated by Britnell *et al.* (2012). Their results showed that hBN layers fulfill all requirements for a most favorable tunnel barrier (Jönsson-Åkerman *et al.*, 2000): (1) It has nonlinear but symmetric *I-V* dependence, (2) such dependence is weakly sensitive to temperature, (3) the resistance of the barrier depends exponentially on thickness, and (4) it is pinhole free. Reported spin valve devices to date have utilized monolayers of exfoliated or CVD-grown hBN, which have comparable resistance with the graphene channel itself (Yamaguchi *et al.*, 2013; Fu *et al.*, 2014; Kamalakar, Dankert *et al.*, 2015; Gurram *et al.*, 2016). Therefore, most of these devices are within the conductivity mismatch range and do not take full advantage of hBN as a tunnel barrier. Device-to-device variations were also observed (Kamalakar, Dankert *et al.*, 2015); see Fig. 10(c). As a different approach, Friedman *et al.* (2014, 2015) used chemically functionalized graphene as a tunnel barrier. From the nonlocal spin valve measurements, they achieved spin injection efficiencies of up to 45% and 17% at low temperatures for fluorinated and hydrogenated graphene-based tunnel barriers, respectively. However, calculated spin-relaxation times in these devices are less than 0.2 ns and the created spin accumulation is extremely small or even absent at room temperature (Friedman *et al.*, 2016). Recently Gurram, Omar, and van Wees (2017) observed bias-induced enhanced spin injection and detection efficiencies up to 100% in tunnel junctions with bilayer hBN barriers. Similar results were obtained for trilayer hBN tunnel barriers (Leutenantsmeyer, Ingla-Aynés, Gurram, and van Wees, 2018). These results are not yet understood.

C. Alternative spin injection and detection techniques

Besides the use of electrical and optical means, ferromagnetic resonance spin pumping has been utilized to inject spins into graphene. In this technique, a ferromagnet is placed in contact with graphene and the magnetization of the ferromagnet is driven into resonant precession with the use of an oscillating magnetic field. The angular-momentum transfer from the precessing ferromagnet drives a spin current into graphene, while this spin transfer is observed as an enhanced damping of the ferromagnetic resonance. Unlike the electrical spin injection method, this dynamical method does not require any tunnel barrier as it allows injection via transparent interfaces. Patra *et al.* (2012) reported the first evidence of spin pumping into chemically grown graphene by demonstrating a broadening of the ferromagnetic resonance absorption peak in Py/graphene and Co/graphene films. The significant absorption of angular momentum suggested that SOC strength in proximitized CVD graphene is larger than for pristine graphene (Patra *et al.*, 2012; Singh *et al.*, 2013). Still, the exclusive use of ferromagnetic broadening to quantify spin

injection was cautioned against by Berger *et al.* (2014), who demonstrated that cobalt grown on graphene has enhanced magnetic disorder; hence, the observed broadening may have a contribution from the structural change of the ferromagnet. This uncertainty was addressed by Tang *et al.* (2013), who unambiguously proved dynamical spin injection at room temperature by detecting the injected spin current via the ISHE in Pd electrodes. A similar approach was later shown using the ISHE of graphene itself (Ohshima *et al.*, 2014). Similar to ISHE, there are other methods for electrically probing spin transport in graphene. Detailed quantum-interference measurements, combining weak localization and universal conductance fluctuations, probed decoherence in graphene (Lundeberg *et al.*, 2013) and indicated that magnetic defects are the dominating source of spin scattering. This identification of an extrinsic source of spin relaxation in the form of magnetic defects is in agreement with later theoretical predictions (Kochan *et al.*, 2015) and spin valve measurements (Avsar *et al.*, 2016).

The unique electronic structure of graphene paves the way for unconventional ways to detect and create spin transport, even without using magnetic contacts. Under a large applied magnetic field, graphene devices in a Hall bar geometry exhibit a large nonlocal resistance (Abanin *et al.*, 2011). This phenomenology, similar to that of the SHE, was attributed to the creation of spin-up electrons and spin-down holes due to Zeeman splitting near the charge neutrality point, without any role for SOC (Abanin, Gorbachev *et al.*, 2011). Further work indicated that thermoelectric effects, i.e., the interaction between thermal and electronic transport, could have a contribution to this nonlocal signal as well (Renard, Studer, and Folk, 2014). The insight that thermoelectric transport is interrelated with spin transport has developed in recent years into the active subfield of spin caloritronics (Bauer, Saitoh, and van Wees, 2012). This interrelation was demonstrated in graphene via the detection of spin currents without the use of magnetic contacts (Vera-Marun, Ranjan, and van Wees, 2012), where the spin-to-charge conversion mechanism relies on the energy-dependent transmission of graphene, the same principle as that of the thermoelectric Seebeck effect (Vera-Marun, Ranjan, and van Wees, 2011). Such a spin-to-charge conversion proved to be a general phenomenon, advantageous for detecting spin transport in mesoscopic systems (Stano, Fabian, and Jacquod, 2012; Yang, Sun, and Xie, 2014; Rameshti and Moghaddam, 2015). More recently the role of thermal gradients on the modulation of spin signals was also demonstrated (Sierra *et al.*, 2018). Graphene and related 2D materials are fundamentally interesting systems for the exploration of novel spin injection and detection approaches, in particular, within the still young subfield of 2D spin caloritronics. Finally, one-dimensional ferromagnetic edge contacts to graphene have started to be explored for spin injection and detection (Guarochico *et al.*, 2017; Karpiak *et al.*, 2017; Xu, Singh *et al.*, 2018). In this regard, graphene in direct contact to a ferromagnet enables the study of an electrically tunable magnetic proximity-induced spin polarization (Lazić, Belashchenko, and Žutić, 2016; Asshoff *et al.*, 2017), which is a promising functionality for future graphene-based spin logic devices (Dery *et al.*, 2012).

D. Vertical junctions for spin memories

Several 2D crystals, including graphene, hBN, and MoS_2, have been integrated into vertical GMR and TMR structures as nonmagnetic barriers (Cobas *et al.*, 2012, 2013; Chen *et al.*, 2013; Iqbal *et al.*, 2013; Meng *et al.*, 2013; Godel *et al.*, 2014; Li *et al.*, 2014; Dankert *et al.*, 2015; Weiyi Wang *et al.*, 2015). These structures are the most prominent class of spintronic devices, widely used as magnetic sensors. Other implementations include uses of graphene as a barrier for spin injection into semiconductors (van 't Erve *et al.*, 2012), to prevent oxidation of ferromagnetic electrodes (Bruno Dlubak *et al.*, 2012), and as a spin-conserving channel in a hot-electron transistor (Banerjee, van der Wiel, and Jansen, 2010).

Interest in the integration of 2D crystals in vertical structures was driven by the prediction that few-layer graphene could act as a perfect spin filter (Karpan *et al.*, 2007, 2008; Yazyev and Pasquarello, 2009). Improved advancements in device fabrication have permitted the study of the nature of magnetoresistance in graphene and hBN-based vertical devices, evidencing the role of charge transfer and proximity effects. The latter include the spin splitting induced in graphene due to proximity to the ferromagnetic electrodes (Asshoff *et al.*, 2017), and for identifying the role of individual resonant defect states in hBN to enhance TMR (Asshoff *et al.*, 2018). All of these approaches give the prospect of engineering vertical magnetoresistance in 2D-based junctions, which are the key elements within current memory architectures of magnetic random access memories (Parkin *et al.*, 2003).

E. Electric-field effect in monolayer and bilayer graphene

As discussed previously, hBN has also been employed to develop device concepts that could pave the way for new types of spin-based logic transistors. In a dual-gated device architecture utilizing hBN as a dielectric layer, Ingla-Aynés, Meijerink, and van Wees (2016) controlled the propagation of spin current at room temperature using the drift of electron spins, as shown in Fig. 11(a). Here the spin-relaxation length of 7.7 μm was demonstrated to be controlled from 0.6 to 90 μm when a dc current of ± 90 μA was applied. Depending on the polarity of the dc current, directional control of spin transport was achieved. This spin drift effect demonstrated how longitudinal electric fields can guide and extend the propagation of spin current.

A similar dual-gated structure, this time using bilayer graphene, was also employed to study a different phenomenon: the role of perpendicular electric fields. Here a transport gap was induced on bilayer graphene by the application of a vertical electric field at low temperature, which allowed a purely electrostatic control of spin current propagation (Avsar *et al.*, 2016). In an entirely opposite trend to the device resistance, the spin signal near the charge neutrality point was observed to rapidly decrease as the displacement field was increased, and eventually the signal became undetectable. This device therefore served as an spin-transport analogy to the charge-based field-effect transistor, demonstrating a full electrostatic-gate control of spin current propagation; see Fig. 11(b). Furthermore, the unique spin-valley coupled band structure of bilayer graphene in such a dual-gated device

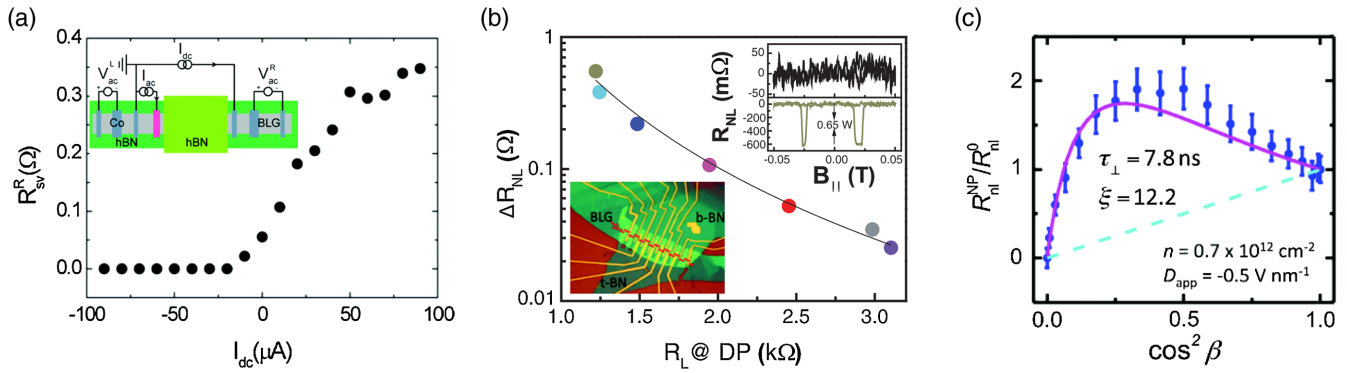

FIG. 11. Electric-field-dependent spin transport in 2D-based heterostructures. (a) The amplitude of the detected spin signal as a function of drift current, demonstrating spin drift. (Inset) The measurement geometry. From Ingla-Aynés, Meijerink, and van Wees, 2016. (b) Dependence of nonlocal spin signal in bilayer graphene on the local resistance at the Dirac point. The latter increases with the vertical electric field, from the yellow (top) to the purple (bottom) dot. At higher fields, the spin current is switched off by the gapped channel. (Top inset) Spin valve measurements at zero (dark yellow line, bottom panel) and high (black line, top panel) displacement fields, demonstrating a spin switch effect. From Avsar *et al.*, 2016. (c) Oblique Hanle measurements near the charge neutrality point in a bilayer-graphene spin valve for different β angles relative to the graphene plane. The magenta solid curve is a fit to the experimental data (blue points with error bars) and reveals an anisotropy of ∼12 in the spin-relaxation time. Away from the charge neutrality point, the anisotropy diminishes and the response becomes similar to the cyan dashed line. From Xu, Zhu *et al.*, 2018.

architecture enables the possibility of modulating the spin-lifetime anisotropy. By performing Hanle spin precession measurements under obliquely oriented magnetic fields, Xu, Zhu *et al.* (2018) demonstrated that the ratio between out-of-plane (7.8 ns) and in-plane (0.64 ns) spin lifetimes is as large as ∼12 near the charge neutrality point, as shown in Fig. 8(c). Such a large anisotropy is the result of an out-of-plane spin-orbit field originating from the induced band gap in bilayer graphene. When increasing the carrier concentration under a fixed vertical displacement field, the in-plane and out-of-plane spin lifetimes eventually become comparable, and therefore the anisotropy disappears. These groundbreaking results, which offer a novel approach to manipulating spin information, were independently demonstrated by Leutenantsmeyer, Ingla-Aynés, Fabian, and van Wees (2018) as well.

F. Proximity-enabled graphene-TMDC novel devices

The ability to control both the flow of spin information and the anisotropy of the spin lifetime via an electrostatic gate in bilayer graphene relies on the presence of its band gap, which is evident only in experiments at low temperature. On the other hand, a similar electrostatic control of spin information was recently realized at room temperature, by exploring graphene-TMDC heterostructures. Electric-field-controlled spin current in graphene/MoS_2 spin valve devices was first reported as a result of gate-tunable spin absorption into the adjacent MoS_2 layer (Yan *et al.*, 2016; Dankert and Dash, 2017); see Fig. 12(a). Later, two independent groups demonstrated that strong spin-valley coupling in WS_2 or MoS_2 results in a change of over 1 order of magnitude between the spin lifetimes for in-plane and out-of-plane spins (Ghiasi *et al.*, 2017; Benítez *et al.*, 2018) [see Figs. 12(b) and 12(c)], which is in good agreement with earlier theoretical predictions (Cummings *et al.*, 2017). These encouraging results in heterostructure systems enabled further theoretical investigations focusing on converting charge current into spin current, using either the SHE that can be induced via proximity in graphene (Garcia, Cummings, and Roche, 2017; Milletarì *et al.*, 2017) or the Rashba-Edelstein effect (REE) present at the graphene-TMDC interface (Offidani *et al.*, 2017). The corresponding inverse effects (ISHE and IREE) are also possible, leading to a reciprocal spin-to-charge conversion.

Toward this direction, Safeer *et al.* (2019) studied graphene/MoS_2 heterostructures and demonstrated the presence of a proximity-induced ISHE in graphene, with an additional spin-to-charge conversion mechanism that could be indistinguishably attributed to either a proximity-induced IREE in graphene or ISHE within the MoS_2 layer; see Fig. 12(d). Soon thereafter, charge-to-spin conversion due to REE in a graphene-monolayer WS_2 heterostructure was demonstrated, also evidencing its carrier density and temperature dependences (Benítez *et al.*, 2019; Ghiasi *et al.*, 2019). Similarly, REE at room temperature was also observed in graphene/TaS_2 (Li *et al.*, 2019) and graphene/$MoTe_2$ (Hoque *et al.*, 2019) heterostructures, with these works also demonstrating the carrier density dependence of the REE efficiency and polarity in agreement with theoretical predictions (Offidani *et al.*, 2017). These recent experiments unambiguously proved charge-to-spin conversion via proximity-induced effects (SHE, REE) by combining Hall probes with standard ferromagnetic electrodes within the same device architecture. The latter is a critical advancement compared to the earlier proximity studies, which utilized only Hall bar (nonmagnetic) electrodes (Avsar *et al.*, 2014; Zhiyong Wang *et al.*, 2015).

G. Spintronics with 2D semiconductors and 2D magnets

Spintronics in 2D semiconductor materials such as black phosphorus (BP) and TMDCs can offer functionality that is not possible when using only graphene, for example, gate-controlled amplification or switching actions. Toward this, Avsar, Tan *et al.* (2017) demonstrated all electrical spin

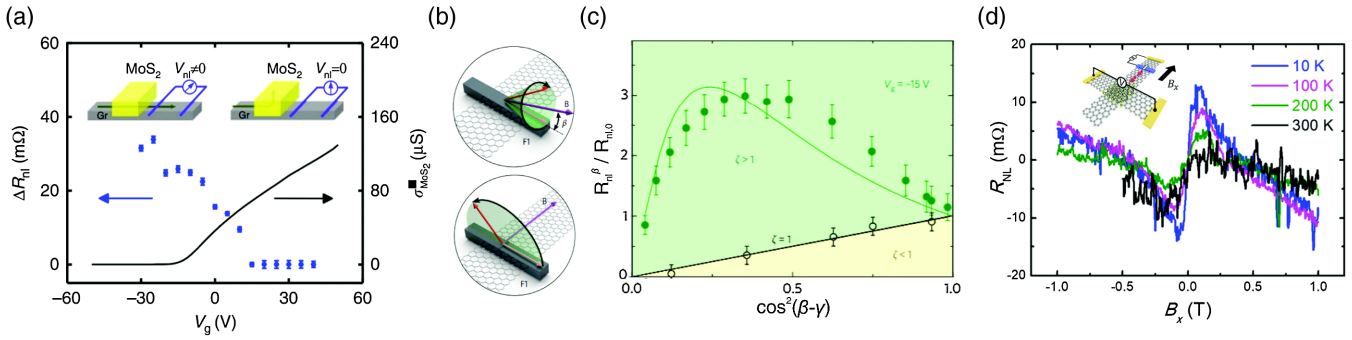

FIG. 12. Proximity-enabled graphene-TMDC devices. (a) Nonlocal spin signal and conductivity for a graphene/MoS_2 device, demonstrating a field-controlled spin absorption. From Yan *et al.*, 2016. (b) The top schematic shows the spin precession cone under an oblique magnetic field, applied in a plane that contains the easy axis of the ferromagnetic electrodes and that is perpendicular to the substrate. The bottom schematic shows the spin precession with magnetic field applied in plane and perpendicular to the easy axis of the ferromagnets. Here the spin precesses on a plane perpendicular to the substrate. From Benítez *et al.*, 2018. (c) Anisotropy measurements in a graphene/WS_2 spin valve device. Solid green dots represent the measurements taken at $V_{BG} = -15$ V, with the green line being a fit revealing an anisotropy of ∼10. The open black dot shows data acquired in a reference graphene spin valve without WS_2 and lacking any anisotropy. From Benítez *et al.*, 2018. (d) Spin-to-charge conversion in a Hall bar detector within a graphene/MoS_2 heterostructure at different temperatures. (Inset) The measurement configuration. From Safeer *et al.*, 2019.

injection, transport, manipulation, and detection in ultrathin BP-based spin valves at room temperature. Based on four-terminal Hanle spin precession measurements, spin relaxation times up to 4.5 ns with spin-relaxation lengths exceeding 6 μm were extracted; see Fig. 13(a). Temperature and gate voltage dependences for spin and momentum relaxation times were in good agreement with first-principles calculations, showing that Elliott-Yafet relaxation is dominant in BP (Li and Appelbaum, 2014; Kurpas, Gmitra, and Fabian, 2016). Further work is required to explore other spintronic properties, like directional spin transport in this anisotropic crystal.

Initial efforts to investigate magnetism in 2D materials focused mostly on proximity-induced (Zhiyong Wang *et al.*, 2015) and defect-induced (Yazyev and Helm, 2007) magnetism. Based on the Mermin-Wagner theorem (Mermin and Wagner, 1966), intrinsic ferromagnetic order is indeed not expected in 2D single layers. This was initially supported by the experimental results obtained from 2D $Cr_2Ge_2Te_6$ where magnetism is absent in its monolayer, at least down to the lowest studied temperatures (4.7 K) (Gong *et al.*, 2017). In this material ferromagnetic order persists nonetheless down to the bilayer, but the critical temperature significantly decreases from 68 (bulk) to 30 K (bilayer), which can be explained by the thermal excitation of the spin waves.

On the other hand, the Mermin-Wagner restriction can be lifted if a material displays strong SOC and magnetocrystalline anisotropy. As shown in Fig. 13(b), layer-dependent magnetic ordering in CrI_3 was demonstrated down to the monolayer thickness, with its spins constrained to lie vertical to the lattice plane as described by the Ising model (Huang

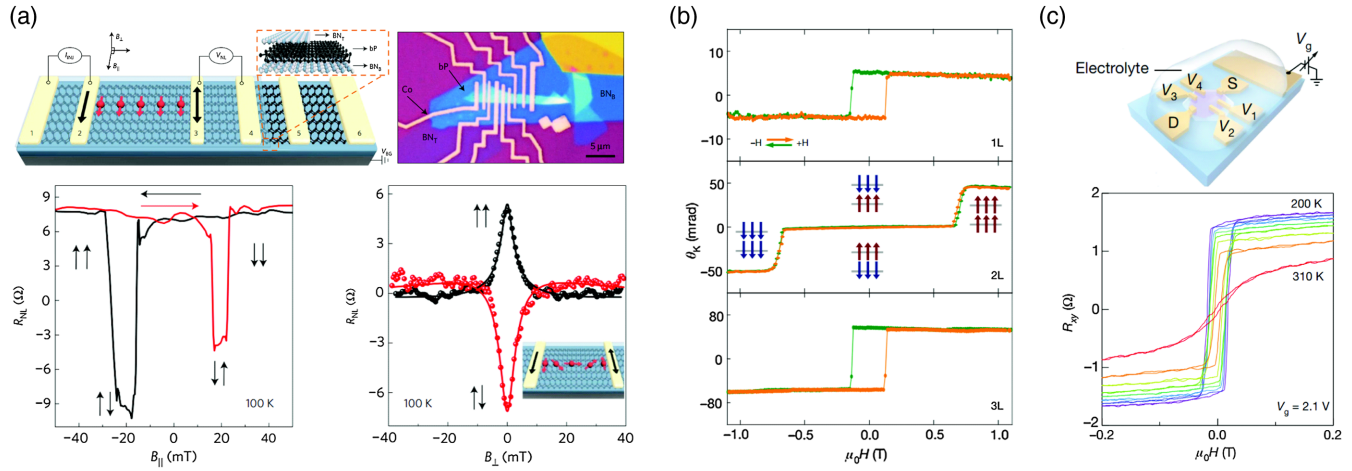

FIG. 13. Spintronics in 2D materials beyond graphene. (a) Spin transport in black phosphorus spin valves. (Top panels) The device schematics and the optical image of a completed device, respectively. (Bottom panels) Spin valve and spin precession curves, respectively, taken at 100 K. From Avsar, Tan *et al.*, 2017. (b) Polar magneto-optical measurement for CrI_3 showing hysteresis for a ferromagnetic monolayer (1L) and trilayer (3L), and vanishing Kerr rotation for an antiferromagnetic bilayer (2L). From Huang *et al.*, 2017. (c) (Top panel) The device geometry, where the electrolyte gating technique was employed to induce an electric field. This tunes the density of states in magnetic Fe_3GeTe_2. (Bottom panel) The anomalous Hall effect measurements as a function of temperature in a four layer thick Fe_3GeTe_2. From Deng *et al.*, 2018.

et al., 2017). The layered structure of CrI_3 provides interesting opportunities: an odd number of layers results in long-range ferromagnetic ordering, while an even number of layers are antiferromagnetic. In the bilayer case, application of an external magnetic field above the coercive field makes the material ferromagnetic; all layers are aligned in the same direction. By taking advantage of this polarization switch, large tunneling magnetoresistance was demonstrated in vertically studied samples (Klein *et al.*, 2018; Song *et al.*, 2018; Wang *et al.*, 2018). At constant voltage bias, such magnetoresistance changes the current by nearly 1×10^6 percent if thicker CrI_3 is employed (Kim *et al.*, 2018). It was also demonstrated that the critical field required to switch from antiferromagnetism to ferromagnetism depends on the vertically applied electric field; see Fig. 13(c) (Huang *et al.*, 2018; Jiang *et al.*, 2018).

Demonstration of 2D magnetism in $Cr_2Ge_2Te_6$ and CrI_3 has resulted in rapid progress toward the discovery of new 2D magnetic materials, such as $CrBr_3$ (Ghazaryan *et al.*, 2018), Fe_3GeTe_2 (Deng *et al.*, 2018), and VSe_2 (Bonilla *et al.*, 2018). Based on magneto-optical measurements, it was shown that VSe_2 shows ferromagnetic ordering persisting up to room temperature in its monolayer, in sharp contrast to its bulk counterpart, which is paramagnetic. Similarly, room-temperature magnetic ordering was discovered in metallic Fe_3GeTe_2 crystals by employing the ionic gating technique. The use of room-temperature 2D magnets for potential spintronic applications is further enabled by their growth using molecular beam epitaxy techniques down to monolayer thickness, as was demonstrated for $MnSe_2$ (O'Hara *et al.*, 2018). Room-temperature spintronic devices could integrate the spin-transport properties of graphene with the memory of the 2D magnet, exploiting proximity-induced magnetization by the 2D magnet into graphene as demonstrated via the proximity anisotropic magnetoresistance effect in graphene/CrB_3 heterostructures (Ghazaryan *et al.*, 2018). Recent observation of defect-induced long-range magnetism in air-stable, metallic $PtSe_2$ (Avsar *et al.*, 2019) and semiconducting $MoTe_2$ (Guguchia *et al.*, 2018) expands the range of 2D magnets into materials that are intrinsically nonmagnetic and would otherwise be overlooked. The emerging mix of experimental techniques and new materials, and the resulting new effects like gate-tunable magnetism, creates prospects for 2D-based voltage-controlled magnetoelectronics.

IV. CONCLUSIONS

Since the first demonstration of spin transport in graphene (Tombros *et al.*, 2007), we have seen significant progress in 2D-based spintronics, including graphene-related materials, getting tantalizingly close to practical applications. This includes, but is not limited to, a 2 order of magnitude enhancement in graphene spin lifetime (Drögeler *et al.*, 2016), high-quality spin transport in large-scale graphene fabricated on conventional Si/SiO_2 (Avsar *et al.*, 2011; Kamalakar, Groenveld *et al.*, 2015; Gebeyehu *et al.*, 2019) and flexible polymer (Serrano *et al.*, 2019) substrates, gate-induced spin manipulation in 2D semiconductors (Avsar, Tan *et al.*, 2017) and graphene-TMDC heterostructures (Yan *et al.*, 2016; Dankert and Dash, 2017), proximity-induced spin-to-charge conversion in graphene-TMDC heterostructures (Ghiasi *et al.*, 2019; Li *et al.*, 2019; Safeer *et al.*, 2019), and the recent discovery of 2D magnets that can even remain magnetically ordered down to a few atoms thick at room temperature (Deng *et al.*, 2018).

However, there are long-standing challenges that need to be addressed to exploit the full potential of 2D spintronics applications. There is still room for improving spin lifetime and spin-relaxation length by studying fully encapsulated, high mobility graphene spin valves. We believe that there are two major breakthroughs to expect when these devices reach the electronic quality of state-of-the-art charge-based devices. First, experimental results in such high-quality spintronic devices will guide the theory to convincingly identify the limiting spin-relaxation mechanisms. Second, analogous to the demonstration of micrometer-scale ballistic charge transport at room temperature (Mayorov *et al.*, 2011), the realization of ballistic spin transport at room temperature could open a whole new range of opportunities. The latter relates both to applications [enabled by spin pumping (Bercioux *et al.*, 2012) or spin filtering (Valli *et al.*, 2018) effects] and to developing a theoretical description to interpret the role of device geometry, spin precession, and transport in a regime beyond the diffusive approximation (Bercioux and De Martino, 2010; Vila *et al.*, 2019). Considering that the field was created only over a decade ago and also its current progress, the vision of low-power all-spin-logic devices based on 2D van der Waals heterostructures seems to be within reach in the coming decade.

ACKNOWLEDGMENTS

We thank D. Bercioux, J. Fabian, A. Ferreira, M. V. Kamalakar, A. G. Moghaddam, S. Roche, E. Sherman, S. O. Valenzuela, and I. Žutić, for the valuable discussions. A. A. thanks A. Ciarrocchi and J. F. G. Marin for the help with the preparation of Fig. 1. B. J. v. W. acknowledges the support from the Zernike Institute for Advanced Materials, and the Spinoza Prize, awarded by the Netherlands Organisation for Scientific Research (NWO). B. Ö. acknowledges support from the National Research Foundation, Prime Ministers Office, Singapore, under its NRF Investigatorship (Grant No. NRF-NRFI2018-08) and the Medium-Sized Centre Programme. I. J. V.-M. acknowledges the support of the Future and Emerging Technologies (FET) Programme within the Seventh Framework Programme for Research of the European Commission, under FET-Open Grant No. 618083 (CNTQC). We acknowledge the financial support from the European Union's Horizon 2020 research and innovation program under Grant Agreements No. 696656 and No. 785219 (Graphene Flagship Cores 1 and 2).

REFERENCES

Abanin, D. A., R. V. Gorbachev, K. S. Novoselov, A. K. Geim, and L. S. Levitov, 2011, "Giant Spin-Hall Effect Induced by the Zeeman Interaction in Graphene," Phys. Rev. Lett. **107**, 096601.

Abanin, D. A., *et al.*, 2011, "Giant nonlocality near the Dirac point in graphene," Science **332**, 328–330.

Abdelouahed, S., A. Ernst, J. Henk, I. V. Maznichenko, and I. Mertig, 2010, "Spin-split electronic states in graphene: Effects due to lattice deformation, Rashba effect, and adatoms by first principles," Phys. Rev. B **82**, 125424.

Alsharari, Abdulrhman M., Mahmoud M. Asmar, and Sergio E. Ulloa, 2016, "Mass inversion in graphene by proximity to dichalcogenide monolayer," Phys. Rev. B **94**, 241106(R).

Asshoff, P. U., *et al.*, 2017, "Magnetoresistance of vertical Co-graphene-NiFe junctions controlled by charge transfer and proximity-induced spin splitting in graphene," 2D Mater. **4**, 031004.

Asshoff, Pablo U., Jose L. Sambricio, Sergey Slizovskiy, Aidan P. Rooney, Takashi Taniguchi, Kenji Watanabe, Sarah J. Haigh, Vladimir Fal'ko, Irina V. Grigorieva, and Ivan J. Vera-Marun, 2018, "Magnetoresistance in Co-hBN-NiFe tunnel junctions enhanced by resonant tunneling through single defects in ultrathin hBN barriers," Nano Lett. **18**, 6954–6960.

Avsar, A., *et al.*, 2014, "Spin-orbit proximity effect in graphene," Nat. Commun. **5**, 4875.

Avsar, Ahmet, Alberto Ciarrocchi, Michele Pizzochero, Dmitrii Unuchek, Oleg V. Yazyev, and Andras Kis, 2019, "Defect induced, layer-modulated magnetism in ultrathin metallic $PtSe_2$," Nat. Nanotechnol. **14**, 674.

Avsar, Ahmet, Jong Hak Lee, Gavin Kok Wai Koon, and Barbaros Özyilmaz, 2015, "Enhanced spin-orbit coupling in dilute fluorinated graphene," 2D Mater. **2**, 044009.

Avsar, Ahmet, Jun Y. Tan, Kenji Watanabe, Marcin Kurpas, Martin Gmitra, Takashi Taniguchi, Jaroslav Fabian, and Barbaros Özyilmaz, 2017, "Gate-tunable black phosphorus spin valve with nanosecond spin lifetimes," Nat. Phys. **13**, 888–893.

Avsar, Ahmet, Dmitrii Unuchek, Jiawei Liu, Oriol Lopez Sanchez, Kenji Watanabe, Takashi Taniguchi, Barbaros Özyilmaz, and Andras Kis, 2017, "Optospintronics in graphene via proximity coupling," ACS Nano **11**, 11678–11686.

Avsar, Ahmet, Ivan Jesus Vera-Marun, Jun You Tan, Gavin Kok Wai Koon, Kenji Watanabe, Takashi Taniguchi, Shaffique Adam, and Barbaros Özyilmaz, 2016, "Electronic spin transport in dual-gated bilayer graphene," NPG Asia Mater. **8**, e274.

Avsar, Ahmet, *et al.*, 2011, "Toward wafer scale fabrication of graphene based spin valve devices," Nano Lett. **11**, 2363–2368.

Awschalom, D. D., D. Loss, and N. Samarth, 2002, Eds., *Semiconductor Spintronics and Quantum Computation*, NanoScience and Technology (Springer-Verlag, Berlin).

Baibich, M. N., J. M. Broto, A. Fert, F. Nguyen Van Dau, F. Petroff, P. Etienne, G. Creuzet, A. Friederich, and J. Chazelas, 1988, "Giant Magnetoresistance of (001)Fe/(001)Cr Magnetic Superlattices," Phys. Rev. Lett. **61**, 2472.

Balakrishnan, Jayakumar, Gavin Kok Wai Koon, Manu Jaiswal, A. H. Castro Neto, and Barbaros Özyilmaz, 2013, "Colossal enhancement of spin-orbit coupling in weakly hydrogenated graphene," Nat. Phys. **9**, 284–287.

Balakrishnan, Jayakumar, *et al.*, 2014, "Giant spin Hall effect in graphene grown by chemical vapour deposition," Nat. Commun. **5**, 4748.

Banerjee, Tamalika, Wilfred G. van der Wiel, and Ron Jansen, 2010, "Spin injection and perpendicular spin transport in graphite nanostructures," Phys. Rev. B **81**, 214409.

Bauer, Gerrit E. W., Eiji Saitoh, and Bart J. van Wees, 2012, "Spin caloritronics," Nat. Mater. **11**, 391–399.

Behin-Aein, Behtash, Deepanjan Datta, Sayeef Salahuddin, and Supriyo Datta, 2010, "Proposal for an all-spin logic device with built-in memory," Nat. Nanotechnol. **5**, 266–270.

Benítez, L. Antonio, Juan F. Sierra, Williams Savero Torres, Aloïs Arrighi, Frédéric Bonell, Marius V. Costache, and Sergio O. Valenzuela, 2018, "Strongly anisotropic spin relaxation in graphene-transition metal dichalcogenide heterostructures at room temperature," Nat. Phys. **14**, 303.

Benítez, L. Antonio, Williams Savero Torres, Juan F. Sierra, Matias Timmermans, Jose H. Garcia, Stephan Roche, Marius V. Costache, and Sergio O. Valenzuela, 2019, "Tunable room-temperature spin galvanic and spin Hall effects in van der Waals heterostructures," arXiv:1908.07868.

Bercioux, D., and A. De Martino, 2010, "Spin-resolved scattering through spin-orbit nanostructures in graphene spin-resolved scattering through spin-orbit nanostructures in graphene," Phys. Rev. B **81**, 165410.

Bercioux, D., D. F. Urban, F. Romeo, and R. Citro, 2012, "Rashba spin-orbit-interaction-based quantum pump in graphene," Appl. Phys. Lett. **101**, 122405.

Berger, A. J., W. Amamou, S. P. White, R. Adur, Y. Pu, R. K. Kawakami, and P. C. Hammel, 2014, "Magnetization dynamics of cobalt grown on graphene," J. Appl. Phys. **115**, 17C510.

Binasch, G., P. Grünberg, F. Saurenbach, and W. Zinn, 1989, "Enhanced magnetoresistance in layered magnetic structures with antiferromagnetic interlayer exchange," Phys. Rev. B **39**, 4828.

Bir, G. L., A. G. Aronov, and G. E. Pikus, 1975, "Spin relaxation of electrons scattered by holes," Zh. Eksp. Teor. Fiz. **69**, 1382 [Sov. Phys. JETP **42**, 705 (1976)].

Bloch, F., 1946, "Nuclear induction," Phys. Rev. **70**, 460.

Bonilla, Manuel, Sadhu Kolekar, Yujing Ma, Horacio Coy Diaz, Vijaysankar Kalappattil, Raja Das, Tatiana Eggers, Humberto R. Gutierrez, Manh-Huong Phan, and Matthias Batzill, 2018, "Strong room-temperature ferromagnetism in VSe_2 monolayers on van der Waals substrates," Nat. Nanotechnol. **13**, 289–293.

Brey, Luis, 2015, "Spin-orbit coupling in graphene induced by adatoms with outer-shell p orbitals," Phys. Rev. B **92**, 235444.

Britnell, Liam, *et al.*, 2012, "Electron tunneling through ultrathin boron nitride crystalline barriers," Nano Lett. **12**, 1707–1710.

Burkov, A. A., Alvaro S. Núñez, and A. H. MacDonald, 2004, "Theory of spin-charge-coupled transport in a two-dimensional electron gas with Rashba spin-orbit interactions," Phys. Rev. B **70**, 155308.

Calleja, Fabian, *et al.*, 2015, "Spatial variation of a giant spin-orbit effect induces electron confinement in graphene on Pb islands," Nat. Phys. **11**, 43.

Cao, T., *et al.*, 2012, "Valley-selective circular dichroism of monolayer molybdenum disulphide," Nat. Commun. **3**, 887.

Cappelluti, E., R. Roldán, J. A. Silva-Guillén, P. Ordejón, and F. Guinea, 2013, "Tight-binding model and direct-gap/indirect-gap transition in single-layer and multilayer MoS_2," Phys. Rev. B **88**, 075409.

Castro, Eduardo V., K. S. Novoselov, S. V. Morozov, N. M. R. Peres, J. M. B. Lopes dos Santos, Johan Nilsson, F. Guinea, A. K. Geim, and A. H. Castro Neto, 2007, "Biased Bilayer Graphene: Semiconductor with a Gap Tunable by the Electric Field Effect," Phys. Rev. Lett. **99**, 216802.

Castro, Eduardo V., H. Ochoa, M. I. Katsnelson, R. V. Gorbachev, D. C. Elias, K. S. Novoselov, A. K. Geim, and F. Guinea, 2010, "Limits on Charge Carrier Mobility in Suspended Graphene due to Flexural Phonons," Phys. Rev. Lett. **105**, 266601.

Castro Neto, A. H., and F. Guinea, 2009, "Impurity-Induced Spin-Orbit Coupling in Graphene," Phys. Rev. Lett. **103**, 026804.

Castro Neto, A. H., F. Guinea, N. M. R. Peres, K. S. Novoselov, and A. K. Geim, 2009, "The electronic properties of graphene," Rev. Mod. Phys. **81**, 109–162.

Chandni, U., Erik A. Henriksen, and J. P. Eisenstein, 2015, "Transport in indium-decorated graphene," Phys. Rev. B **91**, 245402.

Chappert, Claude, Albert Fert, and Frederic Nguyen Van Dau, 2007, "The emergence of spin electronics in data storage," Nat. Mater. **6**, 813–823.

Chen, Jing-Jing, Jie Meng, Yang-Bo Zhou, Han-Chun Wu, Ya-Qing Bie, Zhi-Min Liao, and Da-Peng Yu, 2013, "Layer-by-layer assembly of vertically conducting graphene devices," Nat. Commun. **4**, 1921.

Cho, Sungjae, Yung-Fu Chen, and Michael S. Fuhrer, 2007, "Gate-tunable graphene spin valve," Appl. Phys. Lett. **91**, 123105.

Cobas, E., A. L. Friedman, O. M. J. van 't Erve, J. T. Robinson, and B. T. Jonker, 2013, "Graphene-based magnetic tunnel junctions," IEEE Trans. Magn. **49**, 4343–4346.

Cobas, Enrique, Adam L. Friedman, Olaf M. J. van't Erve, Jeremy T. Robinson, and Berend T. Jonker, 2012, "Graphene as a tunnel barrier: Graphene-based magnetic tunnel junctions," Nano Lett. **12**, 3000–3004.

Cummings, Aron W., Jose H. Garcia, Jaroslav Fabian, and Stephan Roche, 2017, "Giant Spin Lifetime Anisotropy in Graphene Induced by Proximity Effects," Phys. Rev. Lett. **119**, 206601.

Cysne, T. P., J. H. Garcia, A. R. Rocha, and T. G. Rappoport, 2018, "Quantum Hall effect in graphene with interface-induced spin-orbit coupling," Phys. Rev. B **97**, 085413.

Cysne, Tarik P., Aires Ferreira, and Tatiana G. Rappoport, 2018, "Crystal-field effects in graphene with interface-induced spin-orbit coupling," Phys. Rev. B **98**, 045407.

Dankert, André, and Saroj P. Dash, 2017, "Electrical gate control of spin current in van der Waals heterostructures at room temperature," Nat. Commun. **8**, 16093.

Dankert, André, Mutta Venkata Kamalakar, Johan Bergsten, and Saroj P. Dash, 2014, "Spin transport and precession in graphene measured by nonlocal and three-terminal methods," Appl. Phys. Lett. **104**, 192403.

Dankert, André, M. Venkata Kamalakar, Abdul Wajid, R. S. Patel, and Saroj P. Dash, 2015, "Tunnel magnetoresistance with atomically thin two-dimensional hexagonal boron nitride barriers," Nano Res. **8**, 1357–1364.

Dash, Saroj P., Sandeep Sharma, Ram S. Patel, Michel P. de Jong, and Ron Jansen, 2009, "Electrical creation of spin polarization in silicon at room temperature," Nature (London) **462**, 491–494.

Das Sarma, S., Shaffique Adam, E. H. Hwang, and Enrico Rossi, 2011, "Electronic transport in two-dimensional graphene," Rev. Mod. Phys. **83**, 407.

Datta, Supriyo, and Biswajit Das, 1990, "Electronic analog of the electro-optic modulator," Appl. Phys. Lett. **56**, 665–667.

Dayen, Jean-Francois, Soumya J. Ray, Olof Karis, Ivan J. Vera-Marun, and M. Venkata Kamalakar, 2020, "Two-dimensional van der Waals spinterfaces and magnetic-interfaces," Appl. Phys. Rev. **7**, 011303.

Dean, C. R., *et al.*, 2010, "Boron nitride substrates for high-quality graphene electronics," Nat. Nanotechnol. **5**, 722–726.

Deng, Yujun, *et al.*, 2018, "Gate-tunable room-temperature ferromagnetism in two-dimensional Fe_3GeTe_2," Nature (London) **563**, 94.

Dery, H., H. Wu, B. Ciftcioglu, M. Huang, Y. Song, R. Kawakami, J. Shi, I. Krivorotov, I. Zutic, and L. J. Sham, 2012, "Nanospintronics based on magnetologic gates," IEEE Trans. Electron Devices **59**, 259–262.

Diez, Mathias, and Guido Burkard, 2012, "Bias-dependent D'yakonov-Perel' spin relaxation in bilayer graphene," Phys. Rev. B **85**, 195412.

Dlubak, B., M.-B. Martin, C. Deranlot, K. Bouzehouane, S. Fusil, R. Mattana, F. Petroff, A. Anane, P. Seneor, and A. Fert, 2012, "Homogeneous pinhole free 1 nm Al_2O_3 tunnel barriers on graphene," Appl. Phys. Lett. **101**, 203104.

Dlubak, B., P. Seneor, A. Anane, C. Barraud, C. Deranlot, D. Deneuve, B. Servet, R. Mattana, F. Petroff, and A. Fert, 2010, "Are Al_2O_3 and MgO tunnel barriers suitable for spin injection in graphene?," Appl. Phys. Lett. **97**, 092502.

Dlubak, Bruno, *et al.*, 2012, "Graphene-passivated nickel as an oxidation-resistant electrode for spintronics," ACS Nano **6**, 10930–10934.

Dresselhaus, G., and M. S. Dresselhaus, 1965, "Spin-orbit interaction in graphite," Phys. Rev. **140**, A401.

Dresselhaus, M. S., G. Dresselhaus, and A. Jorio, 2008, *Group Theory: Application to the Physics of Condensed Matter* (Springer, New York).

Drögeler, Marc, Christopher Franzen, Frank Volmer, Tobias Pohlmann, Luca Banszerus, Maik Wolter, Kenji Watanabe, Takashi Taniguchi, Christoph Stampfer, and Bernd Beschoten, 2016, "Spin lifetimes exceeding 12 ns in graphene nonlocal spin valve devices," Nano Lett. **16**, 3533–3539.

Drummond, N. D., V. Zolyomi, and V. I. Fal'ko, 2012, "Electrically tunable band gap in silicene," Phys. Rev. B **85**, 075423.

Dugaev, V. K., E. Ya. Sherman, and J. Barnás, 2011, "Spin dephasing and pumping in graphene due to random spin-orbit interaction," Phys. Rev. B **83**, 085306.

D'yakonov, M. I., 2008, *Spin Physics in Semiconductors* (Springer, New York).

D'yakonov, M. I., and V. I. Perel', 1971, "Spin relaxation of conduction electrons in noncentrosymmetric semiconductors," Fiz. Tverd. Tela (Leningrad) **13**, 3581 [Sov. Phys. Solid State **13**, 3023 (1971)].

D'yakonov, M. I., and V. I. Perel', 1973, "Optical orientation in a system of electrons and lattice nuclei in semiconductors theory," Zh. Eksp. Teor. Fiz. **38**, 362–376 [Sov. Phys. JETP **38**, 177 (1973)].

Elias, D. C., *et al.*, 2009, "Control of graphene's properties by reversible hydrogenation: Evidence for graphane," Science **323**, 610.

Elliot, R. J., 1954, "Theory of the effect of spin-orbit coupling on magnetic resonance in some semiconductors," Phys. Rev. **96**, 266.

Ertler, Christian, Sergej Konschuh, Martin Gmitra, and Jaroslav Fabian, 2009, "Electron spin relaxation in graphene: The role of the substrate," Phys. Rev. B **80**, 041405(R).

Ezawa, Motohiko, 2012, "Valley-Polarized Metals and Quantum Anomalous Hall Effect in Silicene," Phys. Rev. Lett. **109**, 055502.

Fabian, Jaroslav, Alex Matos-Abiague, Christian Ertler, Peter Stano, and Igor Zutic, 2007, "Semiconductor spintronics," Acta Phys. Slovaca **57**, 565.

Feng, Wanxiang, Yugui Yao, Wenguang Zhu, Jinjian Zhou, Wang Yao, and Di Xiao, 2012, "Intrinsic spin Hall effect in monolayers of group-VI dichalcogenides: A first-principles study," Phys. Rev. B **86**, 165108.

Ferreira, Aires, Tatiana G. Rappoport, Miguel A. Cazalilla, and A. H. Castro Neto, 2014, "Extrinsic Spin Hall Effect Induced by Resonant Skew Scattering in Graphene," Phys. Rev. Lett. **112**, 066601.

Fert, Albert, 2008, "Nobel Lecture: Origin, development, and future of spintronics," Rev. Mod. Phys. **80**, 1517–1530.

Flatté, M. E., 2007, "Semiconductor spintronics for quantum computation," in *Manipulating Quantum Coherence in Solid State Systems*, NATO Science Series II: Mathematics, Physics and Chemistry Vol. 244, edited by Michael E. Flatté, and I. Ţifrea (Springer Netherlands, Dordrecht), pp. 1–52.

Flatté, M. E., and G. Vignale, 2001, "Unipolar spin diodes and transistors," Appl. Phys. Lett. **78**, 1273–1275.

Fleurence, A., R. Friedlein, T. Ozaki, H. Kawai, Y. Wang, and Y. Yamada-Takamura, 2012, "Experimental Evidence for Epitaxial Silicene on Diboride Thin Films," Phys. Rev. Lett. **108**, 245501.

Fratini, S., D. Gosálbez-Martínez, P. Merodio Cámara, and J. Fernández-Rossier, 2013, "Anisotropic intrinsic spin relaxation in graphene due to flexural distortions," Phys. Rev. B **88**, 115426.

Friedman, Adam L., Olaf M. J. van 't Erve, Jeremy T. Robinson, Keith E. Whitener, Jr., and Berend T. Jonker, 2016, "Homoepitaxial graphene tunnel barriers for spin transport," AIP Adv. **6**, 056301.

Friedman, Adam L., Olaf M. J. van 't Erve, Connie H. Li, Jeremy T. Robinson, and Berend T. Jonker, 2014, "Homoepitaxial tunnel barriers with functionalized graphene-on-graphene for charge and spin transport," Nat. Commun. **5**, 3161.

Friedman, Adam L., Olaf M. J. van 't Erve, Jeremy T. Robinson, Keith E. Whitener, and Berend T. Jonker, 2015, "Hydrogenated graphene as a homoepitaxial tunnel barrier for spin and charge transport in graphene," ACS Nano **9**, 6747–6755.

Fu, Wangyang, Péter Makk, Romain Maurand, Matthias Bräuninger, and Christian Schönenberger, 2014, "Large-scale fabrication of BN tunnel barriers for graphene spintronics," J. Appl. Phys. **116**, 074306.

Garcia, Jose H., Aron W. Cummings, and Stephan Roche, 2017, "Spin Hall effect and weak antilocalization in graphene/transition metal dichalcogenide heterostructures," Nano Lett. **17**, 5078–5083.

Garcia, Jose H., Marc Vila, Aron W. Cummings, and Stephan Roche, 2018, "Spin transport in graphene/transition metal dichalcogenide heterostructures," Chem. Soc. Rev. **47**, 3359–3379.

Gebeyehu, Z. M., S. Parui, J. F. Sierra, M. Timmermans, M. J. Esplandiu, S. Brems, C. Huyghebaert, K. Garello, M. V. Costache, and S. O. Valenzuela, 2019, "Spin communication over 30 μm long channels of chemical vapor deposited graphene on SiO_2," 2D Mater. **6**, 034003.

Geim, A. K., and I. V. Grigorieva, 2013, "Van der Waals heterostructures," Nature (London) **499**, 419.

Ghazaryan, D., *et al.*, 2018, "Magnon-assisted tunnelling in van der Waals heterostructures based on $CrBr_3$," Nat. Electron. **1**, 344–349.

Ghiasi, Talieh S., Josep Ingla-Aynés, Alexey A. Kaverzin, and Bart J. van Wees, 2017, "Large proximity-induced spin lifetime anisotropy in transition-metal dichalcogenide/graphene heterostructures," Nano Lett. **17**, 7528–7532.

Ghiasi, Talieh S., Alexey A. Kaverzin, Patrick J. Blah, and Bart J. van Wees, 2019, "Charge-to-spin conversion by the Rashba-Edelstein effect in two-dimensional van der Waals heterostructures up to room temperature," Nano Lett. **19**, 5959–5966.

Gmitra, M., S. Konschuh, C. Ertler, C. Ambrosch-Draxl, and J. Fabian, 2009, "Band-structure topologies of graphene: Spin-orbit coupling effects from first principles," Phys. Rev. B **80**, 235431.

Gmitra, Martin, and Jaroslav Fabian, 2015, "Graphene on transition-metal dichalcogenides: A platform for proximity spin-orbit physics and optospintronics," Phys. Rev. B **92**, 155403.

Gmitra, Martin, and Jaroslav Fabian, 2017, "Proximity Effects in Bilayer Graphene on Monolayer WSe_2: Field-Effect Spin Valley Locking, Spin-Orbit Valve, and Spin Transistor," Phys. Rev. Lett. **119**, 146401.

Gmitra, Martin, Denis Kochan, and Jaroslav Fabian, 2013, "Spin-Orbit Coupling in Hydrogenated Graphene," Phys. Rev. Lett. **110**, 246602.

Gmitra, Martin, Denis Kochan, Petra H'ogl, and Jaroslav Fabian, 2016, "Trivial and inverted Dirac bands and the emergence of quantum spin Hall states in graphene on transition-metal dichalcogenides," Phys. Rev. B **93**, 155104.

Godel, F., M. Venkata Kamalakar, B. Doudin, Y. Henry, D. Halley, and J.-F. Dayen, 2014, "Voltage-controlled inversion of tunnel magnetoresistance in epitaxial nickel/graphene/MgO/cobalt junctions," Appl. Phys. Lett. **105**, 152407.

Gong, Cheng, *et al.*, 2017, "Discovery of intrinsic ferromagnetism in two-dimensional van der Waals crystals," Nature (London) **546**, 265–269.

Gordon, R. A., D. Yang, E. D. Crozier, D. T. Jiang, and R. F. Frindt, 2002, "Structures of exfoliated single layers of WS_2, MoS_2, and $MoSe_2$ in aqueous suspension," Phys. Rev. B **65**, 125407.

Guarochico, Victor, Jose Sambricio, Irina Grigorieva, and Ivan Vera, 2017, "Spintronics in high-quality graphene heterostructures via 1D contacts," in *Bulletin of the American Physical Society*, Vol. 62 (American Physical Society, New Orleans) Chap. 4, p. P42.00001.

Guguchia, Z., *et al.*, 2018, "Magnetism in semiconducting molybdenum dichalcogenides," Sci. Adv. **4**, eaat3672.

Guimarães, M. H. D., P. J. Zomer, J. Ingla-Aynés, J. C. Brant, N. Tombros, and B. J. van Wees, 2014, "Controlling Spin Relaxation in Hexagonal BN-Encapsulated Graphene with a Transverse Electric Field," Phys. Rev. Lett. **113**, 086602.

Guinea, F., 2010, "Spin-orbit coupling in a graphene bilayer and in graphite," New J. Phys. **12**, 083063.

Guinea, F., A. H. Castro Neto, and N. M. R. Peres, 2006, "Electronic states and Landau levels in graphene stacks," Phys. Rev. B **73**, 245426.

Gurram, M., S. Omar, and B. J. van Wees, 2017, "Bias induced up to 100% spin-injection and detection polarizations in ferromagnet/bilayer-hBN/graphene/hBN heterostructures," Nat. Commun. **8**, 248.

Gurram, M., S. Omar, and B. J. van Wees, 2018, "Electrical spin injection, transport, and detection in graphene-hexagonal boron nitride van der Waals heterostructures: Progress and perspectives," 2D Mater. **5**, 032004.

Gurram, M., S. Omar, S. Zihlmann, P. Makk, C. Schönenberger, and B. J. van Wees, 2016, "Spin transport in fully hexagonal boron nitride encapsulated graphene," Phys. Rev. B **93**, 115441.

Haase, P., S. Fuchs, T. Pruschke, H. Ochoa, and F. Guinea, 2011, "Magnetic moments and Kondo effect near vacancies and resonant scatterers in graphene," Phys. Rev. B **83**, 241408(R).

Haldane, F. D. M., 1988, "Model for a Quantum Hall Effect without Landau Levels: Condensed-Matter Realization of the 'Parity Anomaly,'" Phys. Rev. Lett. **61**, 2015.

Han, Wei, and R. K. Kawakami, 2011, "Spin Relaxation in Single-Layer and Bilayer Graphene," Phys. Rev. Lett. **107**, 047207.

Han, Wei, K. M. McCreary, K. Pi, W. H. Wang, Yan Li, H. Wen, J. R. Chen, and R. K. Kawakami, 2012, "Spin transport and relaxation in graphene," J. Magn. Magn. Mater. **324**, 369–381.

Han, Wei, K. Pi, K. M. McCreary, Yan Li, Jared J. I. Wong, A. G. Swartz, and R. K. Kawakami, 2010, "Tunneling Spin Injection into Single Layer Graphene," Phys. Rev. Lett. **105**, 167202.

Hasan, M. Z., and C. L. Kane, 2010, "Colloquium: Topological insulators," Rev. Mod. Phys. **82**, 3045.

Hill, E. W., A. K. Geim, K. Novoselov, F. Schedin, and P. Blake, 2006, "Graphene spin valve devices," IEEE Trans. Magn. **42**, 2694–2696.

Hoque, Anamul Md, Dmitrii Khokhriakov, Bogdan Karpiak, and Saroj P. Dash, 2019, "All-electrical creation and control of giant spin-galvanic effect in 1T-$MoTe_2$/graphene heterostructures at room temperature," arXiv:1908.09367.

Hu, Jun, Jason Alicea, Ruqian Wu, and Marcel Franz, 2012, "Giant Topological Insulator Gap in Graphene with 5*d* Adatoms," Phys. Rev. Lett. **109**, 266801.

Huang, Bevin, *et al.*, 2017, "Layer-dependent ferromagnetism in a van der Waals crystal down to the monolayer limit," Nature (London) **546**, 270–273.

Huang, Bevin, *et al.*, 2018, "Electrical control of 2D magnetism in bilayer CrI_3," Nat. Nanotechnol. **13**, 544–548.

Huang, Chunli, Y. D. Chong, and Miguel A. Cazalilla, 2016, "Direct coupling between charge current and spin polarization by extrinsic mechanisms in graphene," Phys. Rev. B **94**, 085414.

Huertas-Hernando, D., F. Guinea, and A. Brataas, 2006, "Spin-orbit coupling in curved graphene, fullerenes, nanotubes, and nanotube caps," Phys. Rev. B **74**, 155426.

Huertas-Hernando, D., F. Guinea, and Arne Brataas, 2009, "Spin-Orbit-Mediated Spin Relaxation in Graphene," Phys. Rev. Lett. **103**, 146801.

Ingla-Aynés, J., M. H. D. Guimarães, R. J. Meijerink, P. J. Zomer, and B. J. van Wees, 2015, "24 μm spin relaxation length in boron nitride encapsulated bilayer graphene," Phys. Rev. B **92**, 201410.

Ingla-Aynés, Josep, Rick J. Meijerink, and Bart J. van Wees, 2016, "Eighty-eight percent directional guiding of spin currents with 90 μm relaxation length in bilayer graphene using carrier drift," Nano Lett. **16**, 4825–4830.

Inglot, M., V. K. Dugaev, E. Ya. Sherman, and J. Barnaś, 2014, "Optical spin injection in graphene with Rashba spin-orbit interaction," Phys. Rev. B **89**, 155411.

Iqbal, Muhammad Zahir, Muhammad Waqas Iqbal, Jae Hong Lee, Yong Seung Kim, Seung-Hyun Chun, and Jonghwa Eom, 2013, "Spin valve effect of NiFe/graphene/NiFe junctions," Nano Res. **6**, 373–380.

Irmer, Susanne, Tobias Frank, Sebastian Putz, Martin Gmitra, Denis Kochan, and Jaroslav Fabian, 2015, "Spin-orbit coupling in fluorinated graphene," Phys. Rev. B **91**, 115141.

Island, J. O., *et al.*, 2019, "Spin–orbit-driven band inversion in bilayer graphene by the van der Waals proximity effect," Nature (London) **571**, 85.

Jedema, F. J., M. V. Costache, H. B. Heersche, J. J. A. Baselmans, and B. J. van Wees, 2002, "Electrical detection of spin accumulation and spin precession at room temperature in metallic spin valves," Appl. Phys. Lett. **81**, 5162.

Jedema, F. J., A. T. Filip, and B. J. van Wees, 2001, "Electrical spin injection and accumulation at room temperature in an all-metal mesoscopic spin valve," Nature (London) **410**, 345–348.

Jedema, F. J., H. B. Heersche, A. T. Filip, J. J. A. Baselmans, and B. J. van Wees, 2002, "Electrical detection of spin precession in a metallic mesoscopic spin valve," Nature (London) **416**, 713–716.

Jeon, Kun-Rok, Byoung-Chul Min, Il-Jae Shin, Chang-Yup Park, Hun-Sung Lee, Young-Hun Jo, and Sung-Chul Shin, 2011, "Electrical spin accumulation with improved bias voltage dependence in a crystalline CoFe/MgO/Si system," Appl. Phys. Lett. **98**, 262102.

Jeong, Jae-Seung, Jeongkyu Shin, and Hyun-Woo Lee, 2011, "Curvature-induced spin-orbit coupling and spin relaxation in a chemically clean single-layer graphene," Phys. Rev. B **84**, 195457.

Jia, Zhenzhao, Baoming Yan, Jingjing Niu, Qi Han, Rui Zhu, Dapeng Yu, and Xiaosong Wu, 2015, "Transport study of graphene adsorbed with indium adatoms," Phys. Rev. B **91**, 085411.

Jiang, Shengwei, Lizhong Li, Zefang Wang, Kin Fai Mak, and Jie Shan, 2018, "Controlling magnetism in 2D CrI_3 by electrostatic doping," Nat. Nanotechnol. **13**, 549–553.

Jo, Sanghyun, Dong-Keun Ki, Dongchan Jeong, Hu-Jong Lee, and Stefan Kettemann, 2011, "Spin relaxation properties in graphene due to its linear dispersion," Phys. Rev. B **84**, 075453.

Johnson, Mark, and R. H. Silsbee, 1985, "Interfacial Charge-Spin Coupling: Injection and Detection of Spin Magnetization in Metals," Phys. Rev. Lett. **55**, 1790.

Jönsson-Åkerman, B. J., R. Escudero, C. Leighton, S. Kim, Ivan K. Schuller, and D. A. Rabson, 2000, "Reliability of normal-state current-voltage characteristics as an indicator of tunnel-junction barrier quality," Appl. Phys. Lett. **77**, 1870–1872.

Józsa, C., T. Maassen, M. Popinciuc, P. J. Zomer, A. Veligura, H. T. Jonkman, and B. J. van Wees, 2009, "Linear scaling between momentum and spin scattering in graphene," Phys. Rev. B **80**, 241403(R).

Józsa, C., M. Popinciuc, N. Tombros, H. T. Jonkman, and B. J. van Wees, 2008, "Electronic Spin Drift in Graphene Field-Effect Transistors," Phys. Rev. Lett. **100**, 236603.

Józsa, C., M. Popinciuc, N. Tombros, H. T. Jonkman, and B. J. van Wees, 2009, "Controlling the efficiency of spin injection into graphene by carrier drift," Phys. Rev. B **79**, 081402.

Kaloni, T. P., L. Kou, T. Frauenheim, and U. Schwingenschl'ogl, 2014, "Quantum spin Hall states in graphene interacting with WS_2 or WSe_2," Appl. Phys. Lett. **105**, 233112.

Kamalakar, M. Venkata, André Dankert, Johan Bergsten, Tommy Ive, and Saroj P. Dash, 2015, "Enhanced tunnel spin injection into graphene using chemical vapor deposited hexagonal boron nitride," Sci. Rep. **4**, 6146.

Kamalakar, M. Venkata, Christiaan Groenveld, André Dankert, and Saroj P. Dash, 2015, "Long distance spin communication in chemical vapour deposited graphene," Nat. Commun. **6**, 6766.

Kane, C. L., and E. J. Mele, 2005a, "Z_2 Topological Order and the Quantum Spin Hall Effect," Phys. Rev. Lett. **95**, 146802.

Kane, C. L., and E. J. Mele, 2005b, "Quantum Spin Hall Effect in Graphene," Phys. Rev. Lett. **95**, 226801.

Karpan, V. M., G. Giovannetti, P. A. Khomyakov, M. Talanana, A. A. Starikov, M. Zwierzycki, J. van den Brink, G. Brocks, and P. J. Kelly, 2007, "Graphite and Graphene as Perfect Spin Filters," Phys. Rev. Lett. **99**, 176602.

Karpan, V. M., P. A. Khomyakov, A. A. Starikov, G. Giovannetti, M. Zwierzycki, M. Talanana, G. Brocks, J. van den Brink, and P. J. Kelly, 2008, "Theoretical prediction of perfect spin filtering at interfaces between close-packed surfaces of Ni or Co and graphite or graphene," Phys. Rev. B **78**, 195419.

Karpiak, Bogdan, André Dankert, Aron W. Cummings, Stephen R. Power, Stephan Roche, and Saroj P. Dash, 2017, "1D ferromagnetic edge contacts to 2D graphene/h-BN heterostructures," 2D Mater. **5**, 014001.

Katsnelson, M. I., 2007, "Graphene: Carbon in two dimensions," Mater. Today **10**, 20.

Kaverzin, A. A., and B. J. van Wees, 2015, "Electron transport nonlocality in monolayer graphene modified with hydrogen silsesquioxane polymerization," Phys. Rev. B **91**, 165412.

Khoo, Jun Yong, and Leonid Levitov, 2018, "Tunable quantum Hall edge conduction in bilayer graphene through spin-orbit interaction," Phys. Rev. B **98**, 115307.

Khoo, Jun Yong, Alberto F. Morpurgo, and Leonid Levitov, 2017, "On-demand spin-orbit interaction from which-layer tunability in bilayer graphene," Nano Lett. **17**, 7003.

Kim, Hyun Ho, Bowen Yang, Tarun Patel, Francois Sfigakis, Chenghe Li, Shangjie Tian, Hechang Lei, and Adam W. Tsen, 2018, "One million percent tunnel magnetoresistance in a magnetic van der Waals heterostructure," Nano Lett. **18**, 4885–4890.

Klein, D. R., *et al.*, 2018, "Probing magnetism in 2D van der Waals crystalline insulators via electron tunneling," Science **360**, 1218–1222.

Kochan, Denis, and Jaroslav Fabian, 2019, "Breakdown of the Hebel-Slichter effect in superconducting graphene due to the emergence of Yu-Shiba-Rusinov states at magnetic resonant scatterers," arXiv:1902.05474.

Kochan, Denis, Martin Gmitra, and Jaroslav Fabian, 2014, "Spin Relaxation Mechanism in Graphene: Resonant Scattering by Magnetic Impurities," Phys. Rev. Lett. **112**, 116602.

Kochan, Denis, Susanne Irmer, and Jaroslav Fabian, 2017, "Model spin-orbit coupling Hamiltonians for graphene systems," Phys. Rev. B **95**, 165415.

Kochan, Denis, Susanne Irmer, Martin Gmitra, and Jaroslav Fabian, 2015, "Resonant Scattering by Magnetic Impurities as a Model for Spin Relaxation in Bilayer Graphene," Phys. Rev. Lett. **115**, 196601.

Komatsu, Katsuyoshi, Shinya Kasai, Song-Lin Li, Shu Nakaharai, Nobuhiko Mitoma, Mahito Yamamoto, and Kazuhito Tsukagoshi, 2014, "Spin injection and detection in a graphene lateral spin valve using an yttrium-oxide tunneling barrier," Appl. Phys. Express **7**, 085101.

Konschuh, S., M. Gmitra, and J. Fabian, 2010, "Tight-binding theory of the spin-orbit coupling in graphene," Phys. Rev. B **82**, 245412.

Konschuh, S., M. Gmitra, D. Kochan, and J. Fabian, 2012, "Theory of spin-orbit coupling in bilayer graphene," Phys. Rev. B **85**, 115423.

Kormanyos, Andor, Viktor Zolyomi, Neil D. Drummond, Peter Rakyta, Guido Burkard, and Vladimir I. Fal'ko, 2013, "Monolayer MoS_2: Trigonal warping, the γ valley, and spin-orbit coupling effects," Phys. Rev. B **88**, 045416.

Kudin, Konstantin N., Gustavo E. Scuseria, and Boris I. Yakobson, 2001, "C_2f, C_2F, BN, and C nanoshell elasticity from ab initio computations," Phys. Rev. B **64**, 235406.

Kurpas, Marcin, Martin Gmitra, and Jaroslav Fabian, 2016, "Spin-orbit coupling and spin relaxation in phosphorene: Intrinsic versus extrinsic effects," Phys. Rev. B **94**, 155423.

Kurpas, Marcin, Paulo E. Faria Junior, Martin Gmitra, and Jaroslav Fabian, 2019, "Spin-orbit coupling in elemental two-dimensional materials," Phys. Rev. B **100**, 125422.

Landau, L. D., and E. M. Lifshitz, 1977, *Quantum Mechanics*, 3rd ed. (Pergamon Press, Oxford).

Lazić, Predrag, K. D. Belashchenko, and Igor Žutić, 2016, "Effective gating and tunable magnetic proximity effects in two-dimensional heterostructures," Phys. Rev. B **93**, 241401.

Lee, Changgu, Xiaoding Wei, Jeffrey W. Kysar, and James Hone, 2008, "Measurement of the elastic properties and intrinsic strength of monolayer graphene," Science **321**, 385.

Lenz, Lucia, D. F. Urban, and D. Bercioux, 2013, "Rashba spin-orbit interaction in graphene armchair nanoribbons," Eur. Phys. J. B **86**, 502.

Leutenantsmeyer, Johannes Christian, Josep Ingla-Aynés, Jaroslav Fabian, and Bart J. van Wees, 2018, "Observation of Spin-Valley-Coupling-Induced Large Spin-Lifetime Anisotropy in Bilayer Graphene," Phys. Rev. Lett. **121**, 127702.

Leutenantsmeyer, Johannes Christian, Josep Ingla-Aynés, Mallikarjuna Gurram, and Bart J. van Wees, 2018, "Efficient spin injection into graphene through trilayer hBN tunnel barriers," J. Appl. Phys. **124**, 194301.

Li, Lijun, *et al.*, 2019, "Electrical control of the Rashba-Edelstein effect in a graphene/2H-TaS_2 van der Waals heterostructure at room temperature," arXiv:1906.10702.

Li, Pengke, and Ian Appelbaum, 2014, "Electrons and holes in phosphorene," Phys. Rev. B **90**, 115439.

Li, Wan, Lin Xue, H. D. Abruña, and D. C. Ralph, 2014, "Magnetic tunnel junctions with single-layer-graphene tunnel barriers," Phys. Rev. B **89**, 184418.

Lin, Chia-Ching, Ashish Verma Penumatcha, Yunfei Gao, Vinh Quang Diep, Joerg Appenzeller, and Zhihong Chen, 2013, "Spin transfer torque in a graphene lateral spin valve assisted by an external magnetic field," Nano Lett. **13**, 5177–5181.

Locatelli, Andrea, Kevin R. Knox, Dean Cvetko, Tevfik Onur Menteş, Miguel Angel Niño, Shancai Wang, Mehmet B. Yilmaz, Philip Kim, Richard M. Osgood, Jr., and Alberto Morgante, 2010, "Corrugation in exfoliated graphene: An electron microscopy and diffraction study," ACS Nano **4**, 4879.

López-Sancho, M. P., and M. C. Muñoz, 2011, "Intrinsic spin-orbit interactions in flat and curved graphene nanoribbons," Phys. Rev. B **83**, 075406.

Lou, X., C. Adelmann, M. Furis, S. A. Crooker, C. J. Palmstrøm, and P. A. Crowell, 2006, "Electrical Detection of Spin Accumulation at a Ferromagnet-Semiconductor Interface," Phys. Rev. Lett. **96**, 176603.

Lou, Xiaohua, Christoph Adelmann, Scott A. Crooker, Eric S. Garlid, Jianjie Zhang, K. S. Madhukar Reddy, Soren D. Flexner, Chris J. Palmstrom, and Paul A. Crowell, 2007, "Electrical detection of spin transport in lateral ferromagnet-semiconductor devices," Nat. Phys. **3**, 197–202.

Lundeberg, M. B., R. Yang, J. Renard, and J. A. Folk, 2013, "Defect-Mediated Spin Relaxation and Dephasing in Graphene," Phys. Rev. Lett. **110**, 156601.

Luo, Yunqiu Kelly, Jinsong Xu, Tiancong Zhu, Guanzhong Wu, Elizabeth J. McCormick, Wenbo Zhan, Mahesh R. Neupane, and Roland K. Kawakami, 2017, "Opto-valleytronic spin injection in monolayer MoS_2/few-layer graphene hybrid spin valves," Nano Lett. **17**, 3877–3883.

Ma, Dongwei, Zhongyao Li, and Zhongqin Yang, 2012, "Strong spin-orbit splitting in graphene with adsorbed Au atoms," Carbon **50**, 297–305.

Maassen, T., I. J. Vera-Marun, M. H. D. Guimarães, and B. J. van Wees, 2012, "Contact-induced spin relaxation in Hanle spin precession measurements," Phys. Rev. B **86**, 235408.

Mak, Kin Fai, Keliang He, Jie Sahn, and Tony F. Heinz, 2012, "Control of valley polarization in monolayer MoS_2 by optical helicity," Nat. Nanotechnol. **7**, 494.

Mak, Kin Fai, Changgu Lee, James Hone, Jie Shan, and Tony F. Heinz, 2010, "Atomically Thin MoS_2: A New Direct-Gap Semiconductor," Phys. Rev. Lett. **105**, 136805.

Mañes, J. L., F. Guinea, and M. A. H. Vozmediano, 2007, "Existence and topological stability of Fermi points in multi-layered graphene," Phys. Rev. B **75**, 155424.

Marchenko, D., A. Varykhalov, M. R. Scholz, G. Bihlmayer, E. I. Rashba, A. Rybkin, A. M. Shikin, and O. Rader, 2012, "Giant Rashba splitting in graphene due to hybridization with gold," Nat. Commun. **3**, 1232.

Mayorov, Alexander S., *et al.*, 2011, "Micrometer-scale ballistic transport in encapsulated graphene at room temperature," Nano Lett. **11**, 2396–2399.

McCann, Edward, and Vladimir I. Fal'ko, 2006, "Landau-Level Degeneracy and Quantum Hall Effect in a Graphite Bilayer," Phys. Rev. Lett. **96**, 086805.

McCann, Edward, and Vladimir I. Fal'ko, 2012, "$z \to -z$ Symmetry of Spin-Orbit Coupling and Weak Localization in Graphene," Phys. Rev. Lett. **108**, 166606.

McCann, Edward, and Mikito Koshino, 2010, "Spin-orbit coupling and broken spin degeneracy in multilayer graphene," Phys. Rev. B **81**, 241409(R).

McCreary, Kathleen M., Adrian G. Swartz, Wei Han, Jaroslav Fabian, and Roland K. Kawakami, 2012, "Magnetic Moment Formation in Graphene Detected by Scattering of Pure Spin Currents," Phys. Rev. Lett. **109**, 186604.

Meng, Jie, Jing-Jing Chen, Yuan Yan, Da-Peng Yu, and Zhi-Min Liao, 2013, "Vertical graphene spin valve with Ohmic contacts," Nanoscale **5**, 8894–8898.

Mermin, N. D., and H. Wagner, 1966, "Absence of Ferromagnetism or Antiferromagnetism in One- or Two-Dimensional Isotropic Heisenberg Models," Phys. Rev. Lett. **17**, 1133–1136.

Meservey, R., and P. M. Tedrow, 1994, "Spin-polarized electron tunneling," Phys. Rep. **238**, 173–243.

Milletarì, Mirco, and Aires Ferreira, 2016, "Crossover to the anomalous quantum regime in the extrinsic spin Hall effect of graphene," Phys. Rev. B **94**, 201402.

Milletarì, Mirco, Manuel Offidani, Aires Ferreira, and Roberto Raimondi, 2017, "Covariant Conservation Laws and the Spin Hall Effect in Dirac-Rashba Systems," Phys. Rev. Lett. **119**, 246801.

Min, H., J. E. Hill, N. A. Sinitsyn, B. R. Sahu, L. Kleinman, and A. H. MacDonald, 2006, "Intrinsic and Rashba spin-orbit interactions in graphene sheets," Phys. Rev. B **74**, 165310.

Mishchenko, E. G., A. V. Shytov, and B. I. Halperin, 2004, "Spin Current and Polarization in Impure Two-Dimensional Electron Systems with Spin-Orbit Coupling," Phys. Rev. Lett. **93**, 226602.

Moore, J. E., and L. Balents, 2007, "Topological invariants of time-reversal-invariant bandstructures," Phys. Rev. B **75**, 121306(R).

Muramoto, Kazuya, Masashi Shiraishi, Nobuhiko Mitoma, Takayuki Nozaki, Teruya Shinjo, and Yoshishige Suzuki, 2009, "Analysis of degradation in graphene-based spin valves," Appl. Phys. Express **2**, 123004.

Nair, R. R., M. Sepioni, I.-Ling Tsai, O. Lehtinen, J. Keinonen, A. V. Krasheninnikov, T. Thomson, A. K. Geim, and I. V. Grigorieva, 2012, "Spin-half paramagnetism in graphene induced by point defects," Nat. Phys. **8**, 199–202.

Novoselov, K. S., 2011, "Nobel Lecture: Graphene: Materials in the flatland," Rev. Mod. Phys. **83**, 837–849.

Ochoa, H., A. H. Castro Neto, V. I. Fal'ko, and F. Guinea, 2012, "Spin-orbit coupling assisted by flexural phonons in graphene," Phys. Rev. B **86**, 245411.

Ochoa, H., A. H. Castro Neto, and F. Guinea, 2012, "Elliot-Yafet Mechanism in Graphene," Phys. Rev. Lett. **108**, 206808.

Ochoa, Hector, Francesca Finocchiaro, Francisco Guinea, and Vladimir I. Fal'k, 2014, "Spin-valley relaxation and quantum transport regimes in two-dimensional transition-metal dichalcogenides," Phys. Rev. B **90**, 235429.

Offidani, Manuel, Mirco Milletarì, Roberto Raimondi, and Aires Ferreira, 2017, "Optimal Charge-to-Spin Conversion in Graphene on Transition-Metal Dichalcogenides," Phys. Rev. Lett. **119**, 196801.

O'Hara, Dante J., *et al.*, 2018, "Room temperature intrinsic ferromagnetism in epitaxial manganese selenide films in the monolayer limit," Nano Lett. **18**, 3125–3131.

Ohshima, Ryo, Atsushi Sakai, Yuichiro Ando, Teruya Shinjo, Kenji Kawahara, Hiroki Ago, and Masashi Shiraishi, 2014, "Observation of spin-charge conversion in chemical-vapor-deposition-grown single-layer graphene," Appl. Phys. Lett. **105**, 162410.

Pachoud, Alexandre, Aires Ferreira, B. Özyilmaz, and A. H. Castro Neto, 2014, "Scattering theory of spin-orbit active adatoms on graphene," Phys. Rev. B **90**, 035444.

Palacios, J. J., J. Fernández-Rossier, and L. Brey, 2008, "Vacancy-induced magnetism in graphene and graphene ribbons," Phys. Rev. B **77**, 195428.

Parkin, Stuart, Xin Jiang, Christian Kaiser, A. Panchula, K. Roche, and Mahesh Samant, 2003, "Magnetically engineered spintronic sensors and memory," Proc. IEEE **91**, 661–680.

Partoens, B., and F. M. Peeters, 2006, "From graphene to graphite: Electronic structure around the *K* point," Phys. Rev. B **74**, 075404.

Patra, A. K., S. Singh, B. Barin, Y. Lee, J.-H. Ahn, E. del Barco, E. R. Mucciolo, and B. Özyilmaz, 2012, "Dynamic spin injection into chemical vapor deposited graphene," Appl. Phys. Lett. **101**, 162407.

Pereira, Vitor M., F. Guinea, J. M. B. Lopes dos Santos, N. M. R. Peres, and A. H. Castro Neto, 2006, "Disorder Induced Localized States in Graphene," Phys. Rev. Lett. **96**, 036801.

Peres, N. M. R., 2010, "Colloquium: The transport properties of graphene: An introduction," Rev. Mod. Phys. **82**, 2673.

Pesin, Dmytro, and Allan H. MacDonald, 2012, "Spintronics and pseudospintronics in graphene and topological insulators," Nat. Mater. **11**, 409–416.

Popinciuc, M., C. Józsa, P. J. Zomer, N. Tombros, A. Veligura, H. T. Jonkman, and B. J. van Wees, 2009, "Electronic spin transport in graphene field-effect transistors," Phys. Rev. B **80**, 214427.

Qi, X.-L., and S.-C. Zhang, 2011, "Topological insulators and superconductors," Rev. Mod. Phys. **83**, 1057.

Qiao, Zhenhua, Wei Ren, Hua Chen, L. Bellaiche, Zhenyu Zhang, A. H. MacDonald, and Qian Niu, 2014, "Quantum Anomalous Hall Effect in Graphene Proximity Coupled to an Antiferromagnetic Insulator," Phys. Rev. Lett. **112**, 116404.

Qiao, Zhenhua, Shengyuan A. Yang, Wanxiang Feng, Wang-Kong Tse, Jun Ding, Yugui Yao, Jian Wang, and Qian Niu, 2010, "Quantum anomalous Hall effect in graphene from Rashba and exchange effects," Phys. Rev. B **82**, 161414(R).

Rameshti, B. Z., and A. G. Moghaddam, 2015, "Spin-dependent Seebeck effect and spin caloritronics in magnetic graphene," Phys. Rev. B **91**, 155407.

Rashba, E. I., 2000, "Theory of electrical spin injection: Tunnel contacts as a solution of the conductivity mismatch problem," Phys. Rev. B **62**, R16267.

Renard, Julien, Matthias Studer, and Joshua A. Folk, 2014, "Origins of Nonlocality near the Neutrality Point in Graphene," Phys. Rev. Lett. **112**, 116601.

Roche, Stephan, and Sergio O. Valenzuela, 2014, "Graphene spintronics: Puzzling controversies and challenges for spin manipulation," J. Phys. D **47**, 094011.

Roche, Stephan, *et al.*, 2015, "Graphene spintronics: The European Flagship perspective," 2D Mater. **2**, 030202.

Roldán, R., M. P. López-Sancho, E. Cappelluti, J. A. Silva-Guillén, P. Ordejón, and F. Guinea, 2014, "Momentum dependence of spin-orbit interaction effects in single-layer and multi-layer transition metal dichalcogenides," 2D Mater. **1**, 034003.

Rostami, Habib, Ali G. Moghaddam, and Reza Asgari, 2013, "Effective lattice Hamiltonian for monolayer MoS_2: Tailoring electronic structure with perpendicular electric and magnetic fields," Phys. Rev. B **88**, 085440.

Roy, Rahul, 2009, "$\mathbb{Z}_2$ classification of quantum spin Hall systems: An approach using time-reversal invariance," Phys. Rev. B **79**, 195321.

Safeer, C. K., Josep Ingla-Aynés, Franz Herling, José H. Garcia, Marc Vila, Nerea Ontoso, M. Reyes Calvo, Stephan Roche, Luis E. Hueso, and Fèlix Casanova, 2019, "Room-temperature spin Hall effect in graphene/MoS_2 van der Waals heterostructures," Nano Lett. **19**, 1074–1082.

Santos, Flaviano José dos, Dario A. Bahamon, Roberto B. Muniz, Keith McKenna, Eduardo V. Castro, Johannes Lischner, and Aires Ferreira, 2018, "Impact of complex adatom-induced interactions on quantum spin Hall phases," Phys. Rev. B **98**, 081407.

Santos, H., M. C. Muñoz, M. P. López-Sancho, and L. Chico, 2013, "Interplay between symmetry and spin-orbit coupling on graphene nanoribbons," Phys. Rev. B **87**, 235402.

Schuler, Bruno, *et al.*, 2018, "Large spin-orbit splitting of deep in-gap defect states of engineered sulfur vacancies in monolayer WS_2," arXiv:1810.02896.

Seneor, P., B. Dlubak, M.-B. Martin, A. Anane, H. Jaffres, and A. Fert, 2012, "Spintronics with graphene," MRS Bull. **37**, 1245–1254.

Serrano, I. G., J. Panda, Fernand Denoel, Örjan Vallin, Dibya Phuyal, Olof Karis, and M. Venkata Kamalakar, 2019, "Two-dimensional flexible high diffusive spin circuits," Nano Lett. **19**, 666–673.

Shiraishi, Masashi, 2012, "Electrically-generated pure spin current in graphene," Jpn. J. Appl. Phys. **51**, 08KA01.

Shiraishi, Masashi, Megumi Ohishi, Ryo Nouchi, Nobuhiko Mitoma, Takayuki Nozaki, Teruya Shinjo, and Yoshishige Suzuki, 2009, "Robustness of spin polarization in graphene-based spin valves," Adv. Funct. Mater. **19**, 3711–3716.

Sichau, J., M. Prada, T. Anlauf, T. J. Lyon, B. Bosnjak, L. Tiemann, and R. H. Blick, 2019, "Resonance Microwave Measurements of an Intrinsic Spin-Orbit Coupling Gap in Graphene: A Possible Indication of a Topological State," Phys. Rev. Lett. **122**, 046403.

Sierra, Juan F., Ingmar Neumann, Jo Cuppens, Bart Raes, Marius V. Costache, and Sergio O. Valenzuela, 2018, "Thermoelectric spin voltage in graphene," Nat. Nanotechnol. **13**, 107–111.

Singh, Simranjeet, Jyoti Katoch, Jinsong Xu, Cheng Tan, Tiancong Zhu, Walid Amamou, James Hone, and Roland Kawakami, 2016, "Nanosecond spin relaxation times in single layer graphene spin valves with hexagonal boron nitride tunnel barriers," Appl. Phys. Lett. **109**, 122411.

Singh, Simranjeet, Ajit Kumar Patra, Brett Barin, Enrique del Barco, and Barbaros Ozyilmaz, 2013, "Spin pumping in Permalloy/graphene and Permalloy/graphite interfaces," IEEE Trans. Magn. **49**, 3147–3150.

Slonczewski, J. C., and P. R. Weiss, 1958, "Band structure of graphite," Phys. Rev. **109**, 272.

Song, Tiancheng, *et al.*, 2018, "Giant tunneling magnetoresistance in spin-filter van der Waals heterostructures," Science **360**, 1214–1218.

Soriano, David, Dinh Van Tuan, Simon M.-M. Dubois, Martin Gmitra, Aron W. Cummings, Denis Kochan, Frank Ortmann, Jean-Christophe Charlier, Jaroslav Fabian, and Stephan Roche, 2015, "Spin transport in hydrogenated graphene," 2D Mater. **2**, 022002.

Stano, Peter, Jaroslav Fabian, and Philippe Jacquod, 2012, "Nonlinear spin to charge conversion in mesoscopic structures," Phys. Rev. B **85**, 241301.

Tan, J. Y., *et al.*, 2014, "Electronic transport in graphene-based heterostructures," Appl. Phys. Lett. **104**, 183504.

Tang, Zhenyao, Eiji Shikoh, Hiroki Ago, Kenji Kawahara, Yuichiro Ando, Teruya Shinjo, and Masashi Shiraishi, 2013, "Dynamically generated pure spin current in single-layer graphene," Phys. Rev. B **87**, 140401.

Tománek, David, and Steven G. Louie, 1988, "First-principles calculation of highly asymmetric structure in scanning-tunneling-microscopy images of graphite," Phys. Rev. B **37**, 8327.

Tombros, Nikolaos, Csaba Jozsa, Mihaita Popinciuc, Harry T. Jonkman, and Bart J. van Wees, 2007, "Electronic spin transport and spin precession in single graphene layers at room temperature," Nature (London) **448**, 571–574.

Torrey, H. C., 1956, "Bloch equations with diffusion terms," Phys. Rev. **104**, 563.

Tran, M., H. Jaffrès, C. Deranlot, J.-M. George, A. Fert, A. Miard, and A. Lemaître, 2009, "Enhancement of the Spin Accumulation at the Interface between a Spin-Polarized Tunnel Junction and a Semiconductor," Phys. Rev. Lett. **102**, 036601.

Tsang, C. H., R. E. Fontana, T. Lin, D. E. Heim, B. A. Gurney, and M. L. Williams, 1998, "Design, fabrication, and performance of spin-valve read heads for magnetic recording applications," IBM J. Res. Dev. **42**, 103–116.

Tuan, Dinh Van, Frank Ortmann, David Soriano, Sergio O. Valenzuela, and Stephan Roche, 2014, "Pseudospin-driven spin relaxation mechanism in graphene," Nat. Phys. **10**, 857.

Valli, A., A. Amaricci, V. Brosco, and M. Capone, 2018, "Quantum interference assisted spin filtering in graphene nanoflakes," Nano Lett. **18**, 2158.

van Gelderen, Ralph, and C. Morais Smith, 2010, "Rashba and intrinsic spin-orbit interactions in biased bilayer graphene," Phys. Rev. B **81**, 125435.

van 't Erve, O. M. J., A. L. Friedman, E. Cobas, C. H. Li, J. T. Robinson, and B. T. Jonker, 2012, "Low-resistance spin injection into silicon using graphene tunnel barriers," Nat. Nanotechnol. **7**, 737–742.

Van Tuan, D., J. M. Marmolejo-Tejada, X. Waintal, B. K. Nikolić, S. O. Valenzuela, and S. Roche, 2016, "Spin Hall Effect and Origins of Nonlocal Resistance in Adatom-Decorated Graphene," Phys. Rev. Lett. **117**, 176602.

Vera-Marun, I. J., V. Ranjan, and B. J. van Wees, 2011, "Nonlinear interaction of spin and charge currents in graphene," Phys. Rev. B **84**, 241408(R).

Vera-Marun, Ivan J., Vishal Ranjan, and Bart J. van Wees, 2012, "Nonlinear detection of spin currents in graphene with non-magnetic electrodes," Nat. Phys. **8**, 313–316.

Vicent, I. M., H. Ochoa, and F. Guinea, 2017, "Spin relaxation in corrugated graphene," Phys. Rev. B **95**, 195402.

Vila, Marc, Jose H. Garcia, Aron W. Cummings, Stephen R. Power, Christoph Groth, Xavier Waintal, and Stephan Roche, 2019, "Nonlocal spin dynamics in the crossover from diffusive to ballistic transport," arXiv:1910.06194.

Vogt, P., P. De Padova, C. Quaresima, J. Avila, E. Frantzeskakis, M. C. Asensio, A. Resta, B. Ealet, and G. Le Lay, 2012, "Silicene: Compelling Experimental Evidence for Graphenelike Two-Dimensional Silicon," Phys. Rev. Lett. **108**, 155501.

Wang, L., and M. W. Wu, 2014a, "Electron spin relaxation due to D'yakonov-Perel' and Elliot-Yafet mechanisms in monolayer MoS_2: Role of intravalley and intervalley processes," Phys. Rev. B **89**, 115302.

Wang, L., and M. W. Wu, 2014b, "Intrinsic electron spin relaxation due to the D'yakonov-Perel' mechanism in monolayer MoS_2," Phys. Lett. A **378**, 1336.

Wang, Q. H., K. Kalantar-Zadeh, A. Kis, J. N. Coleman, and M. S. Strano, 2012, "Electronics and optoelectronics of two-dimensional transition metal dichalcogenides," Nat. Nanotechnol. **7**, 699.

Wang, W. H., K. Pi, Y. Li, Y. F. Chiang, P. Wei, J. Shi, and R. K. Kawakami, 2008, "Magnetotransport properties of mesoscopic graphite spin valves," Phys. Rev. B **77**, 020402.

Wang, Weiyi, *et al.*, 2015, "Spin-valve effect in NiFe/MoS_2/NiFe junctions," Nano Lett. **15**, 5261–5267.

Wang, Yilin, Xinghan Cai, Janice Reutt-Robey, and Michael S. Fuhrer, 2015, "Neutral-current Hall effects in disordered graphene," Phys. Rev. B **92**, 161411.

Wang, Yilin, Shudong Xiao, Xinghan Cai, Wenzhong Bao, Janice Reutt-Robey, and Michael S. Fuhrer, 2015, "Electronic transport properties of Ir-decorated graphene," Sci. Rep. **5**, 15764.

Wang, Zhe, Ignacio Gutiérrez-Lezama, Nicolas Ubrig, Martin Kroner, Marco Gibertini, Takashi Taniguchi, Kenji Watanabe, Ataç Imamoğlu, Enrico Giannini, and Alberto F. Morpurgo, 2018, "Very large tunneling magnetoresistance in layered magnetic semiconductor CrI_3," Nat. Commun. **9**, 2516.

Wang, Zhe, Dong-Keun Ki, Hua Chen, Helmuth Berger, Allan H. MacDonald, and Alberto F. Morpurgo, 2015, "Strong interface-induced spin-orbit interaction in graphene on WS_2," Nat. Commun. **6**, 8339.

Wang, Zhe, Dong-Keun Ki, Jun Yong Khoo, Diego Mauro, Helmuth Berger, Leonid S. Levitov, and Alberto F. Morpurgo, 2016, "Origin and Magnitude of 'Designer' Spin-Orbit Interaction in Graphene on Semiconducting Transition Metal Dichalcogenides," Phys. Rev. X **6**, 041020.

Wang, Zhiyong, Chi Tang, Raymond Sachs, Yafis Barlas, and Jing Shi, 2015, "Proximity-Induced Ferromagnetism in Graphene Revealed by the Anomalous Hall Effect," Phys. Rev. Lett. **114**, 016603.

Watanabe, K., T. Taniguchi, and H. Kanda, 2004, "Direct-bandgap properties and evidence for ultraviolet lasing of hexagonal boron nitride single crystal," Nat. Mater. **3**, 404.

Weeks, Conan, Jun Hu, Jason Alicea, Marcel Franz, and Ruqian Wu, 2011, "Engineering a Robust Quantum Spin Hall State in Graphene via Adatom Deposition," Phys. Rev. X **1**, 021001.

Wehling, T. O., S. Yuan, A. I. Lichtenstein, A. K. Geim, and M. I. Katsnelson, 2010, "Resonant Scattering by Realistic Impurities in Graphene," Phys. Rev. Lett. **105**, 056802.

Wen, Hua, Hanan Dery, Walid Amamou, Tiancong Zhu, Zhisheng Lin, Jing Shi, Igor Žutić, Ilya Krivorotov, L. J. Sham, and Roland K. Kawakami, 2016, "Experimental Demonstration of XOR Operation in Graphene Magnetologic Gates at Room Temperature," Phys. Rev. Applied **5**, 044003.

Wojtaszek, M., I. J. Vera-Marun, T. Maassen, and B. J. van Wees, 2013, "Enhancement of spin relaxation time in hydrogenated graphene spin-valve devices," Phys. Rev. B **87**, 081402.

Wojtaszek, M., I. J. Vera-Marun, E. Whiteway, M. Hilke, and B. J. van Wees, 2014, "Absence of hyperfine effects in ^{13}C-graphene spin-valve devices," Phys. Rev. B **89**, 035417.

Wolf, S. A., A. Y. Chtchelkanova, and D. M. Treger, 2006, "Spintronics—A retrospective and perspective," IBM J. Res. Dev. **50**, 101–110.

Xia, Fengnian, Han Wang, and Yichen Jia, 2014, "Rediscovering black phosphorus as an anisotropic layered material for optoelectronics and electronics," Nat. Commun. **5**, 4458.

Xiao, D., G.-B. Liu, W. Feng, X. Xu, and W. Yao, 2012, "Coupled Spin and Valley Physics in Monolayers of MoS_2 and Other Group-VI Dichalcogenides," Phys. Rev. Lett. **108**, 196802.

Xu, Jinsong, Simranjeet Singh, Jyoti Katoch, Guanzhong Wu, Tiancong Zhu, Igor Žutić, and Roland K. Kawakami, 2018, "Spin inversion in graphene spin valves by gate-tunable magnetic proximity effect at one-dimensional contacts," Nat. Commun. **9**, 2869.

Xu, Jinsong, Tiancong Zhu, Yunqiu Kelly Luo, Yuan-Ming Lu, and Roland K. Kawakami, 2018, "Strong and Tunable Spin-Lifetime Anisotropy in Dual-Gated Bilayer Graphene," Phys. Rev. Lett. **121**, 127703.

Yafet, Y., 1963, *Solid State Physics* (Academic, New York).

Yamaguchi, Takehiro, Yoshihisa Inoue, Satoru Masubuchi, Sei Morikawa, Masahiro Onuki, Kenji Watanabe, Takashi Taniguchi, Rai Moriya, and Tomoki Machida, 2013, "Electrical spin injection into graphene through monolayer hexagonal boron nitride," Appl. Phys. Express **6**, 073001.

Yamaguchi, Takehiro, Satoru Masubuchi, Kazuyuki Iguchi, Rai Moriya, and Tomoki Machida, 2012, "Tunnel spin injection into graphene using Al_2O_3 barrier grown by atomic layer deposition on functionalized graphene surface," J. Magn. Magn. Mater. **324**, 849–852.

Yan, Wenjing, Oihana Txoperena, Roger Llopis, Hanan Dery, Luis E. Hueso, and Fèlix Casanova, 2016, "A two-dimensional spin field-effect switch," Nat. Commun. **7**, 13372.

Yang, Bowen, Mark Lohmann, David Barroso, Ingrid Liao, Zhisheng Lin, Yawen Liu, Ludwig Bartels, Kenji Watanabe, Takashi Taniguchi, and Jing Shi, 2017, "Strong electron-hole symmetric Rashba spin-orbit coupling in graphene/monolayer transition metal dichalcogenide heterostructures," Phys. Rev. B **96**, 041409(R).

Yang, Bowen, Min-Feng Tu, Jeongwoo Kim, Yong Wu, Hui Wang, Jason Alicea, Ruqian Wu, Marc Bockrath, and Jing Shi, 2016, "Tunable spin-orbit coupling and symmetry-protected edge states in graphene/WS_2," 2D Mater. **3**, 031012.

Yang, T.-Y., *et al.*, 2011, "Observation of Long Spin-Relaxation Times in Bilayer Graphene at Room Temperature," Phys. Rev. Lett. **107**, 047206.

Yang, Zhi-Cheng, Qing-Feng Sun, and X. C. Xie, 2014, "Spin-current Seebeck effect in quantum dot systems," J. Phys. Condens. Matter **26**, 045302.

Yao, Y., F. Ye, X.-L. Qi, S.-C. Zhang, and Z. Fang, 2007, "Spin-orbit gap of graphene: First-principles calculations," Phys. Rev. B **75**, 041401(R).

Yazyev, Oleg V., 2008, "Magnetism in Disordered Graphene and Irradiated Graphite," Phys. Rev. Lett. **101**, 037203.

Yazyev, Oleg V., and Lothar Helm, 2007, "Defect-induced magnetism in graphene," Phys. Rev. B **75**, 125408.

Yazyev, Oleg V., and Alfredo Pasquarello, 2009, "Magnetoresistive junctions based on epitaxial graphene and hexagonal boron nitride," Phys. Rev. B **80**, 035408.

Zakharchenko, K. V., R. Roldán, A. Fasolino, and M. I. Katsnelson, 2010, "Self-consistent screening approximation for flexible membranes: Application to graphene," Phys. Rev. B **82**, 125435.

Zaletel, M. P., and J. Y. Khoo, 2019, "The gate-tunable strong and fragile topology of multilayer-graphene on a transition metal dichalcogenide," arXiv:1901.01294.

Zarea, M., and N. Sandler, 2009, "Rashba spin-orbit interaction in graphene and zigzag nanoribbons," Phys. Rev. B **79**, 165442.

Zeng, H., J. Dai, W. Yao, D. Xiao, and X. Cui, 2012, "Valley polarization in MoS_2 monolayers by optical pumping," Nat. Nanotechnol. **7**, 490.

Zhang, P., and M. W. Wu, 2011, "Electron spin diffusion and transport in graphene," Phys. Rev. B **84**, 045304.

Zhang, P., and M. W. Wu, 2012, "Electron spin relaxation in graphene with random Rashba field: Comparison of the D'yakonov-Perel' and Elliot-Yafel-like mechanisms," New J. Phys. **14**, 033015.

Zhou, Y., and M. W. Wu, 2010, "Electron spin relaxation in graphene from a microscopic approach: Role of electron-electron interaction," Phys. Rev. B **82**, 085304.

Zhu, Z. Y., Y. C. Cheng, and U. Schwingenschlogl, 2011, "Giant spin-orbit-induced spin splitting in two-dimensional transition-metal dichalcogenide semiconductors," Phys. Rev. B **84**, 153402.

Zomer, P. J., M. H. D. Guimarães, N. Tombros, and B. J. van Wees, 2012, "Long-distance spin transport in high-mobility graphene on hexagonal boron nitride," Phys. Rev. B **86**, 161416.

Žutić, Igor, Jaroslav Fabian, and S. Das Sarma, 2004, "Spintronics: Fundamentals and applications," Rev. Mod. Phys. **76**, 323–410.

Žutić, Igor, Jaroslav Fabian, and Steven C. Erwin, 2006, "Spin Injection and Detection in Silicon," Phys. Rev. Lett. **97**, 026602.

Žutić, Igor, Alex Matos-Abiague, Benedikt Scharf, Hanan Dery, and Kirill Belashchenko, 2019, "Proximitized materials," Mater. Today **22**, 85–107.